Dynamic properties of two-dimensional and quasi-geostrophic turbulence

by

Andreas Vallgren

November 2010 Department of Mechanics Royal Institute of Technology SE-100 44 Stockholm, Sweden

Akademisk avhandling som med tillstånd av Kungliga Tekniska Högskolan i Stockholm framlägges till offentlig granskning för avläggande av filosofie doktorsexamen fredagen den 19 november 2010 kl 10.15 i sal D1, Kungliga Tekniska Högskolan, Lindstedtsvägen 17, Stockholm.

©Andreas Vallgren 2010
Universitetsservice US-AB, Stockholm 2010

Dynamic properties of two-dimensional and quasi-geostrophic turbulence

Andreas Vallgren

Linné Flow Centre, Department of Mechanics, Royal Institute of Technology (KTH)

SE-100 44 Stockholm, Sweden

Abstract

Two codes have been developed and implemented for use on massively parallel super computers to simulate two-dimensional and quasi-geostrophic turbulence. The codes have been found to scale well with increasing resolution and width of the simulations. This has allowed for the highest resolution simulations of twodimensional and quasi-geostrophic turbulence so far reported in the literature. The direct numerical simulations have focused on the statistical characteristics of turbulent cascades of energy and enstrophy, the role of coherent vortices and departures from universal scaling laws, theoretized more than 40 years ago. In particular, the investigations have concerned the enstrophy and energy cascades in forced and decaying two-dimensional turbulence. Furthermore, the applicability of Charney's hypotheses on quasi-geostrophic turbulence has been tested. The results have shed light on the flow evolution at very large Reynolds numbers. The most important results are the robustness of the enstrophy cascade in forced and decaying two-dimensional turbulence, the sensitivity to an infrared Reynolds number in the spectral scaling of the energy spectrum in the inverse energy cascade range, and the validation of Charney's predictions on the dynamics of quasi-geostrophic turbulence. It has also been shown that the scaling of the energy spectrum in the enstrophy cascade is insensitive to intermittency in higher order statistics, but that corrections apply to the "universal" Batchelor-Kraichnan constant, as a consequence of large-scale dissipation anomalies following a classical remark by Landau (Landau & Lifshitz 1987). Another finding is that the inverse energy cascade is maintained by nonlocal triad interactions, which is in contradiction with the classical locality assumption.

Descriptors: two-dimensional turbulence, decaying turbulence, quasi-geostrophic turbulence, direct numerical simulation (DNS), coherent vortices, energy cascade, enstrophy cascade, intermittency, massively parallel simulations, locality

Preface

This thesis investigates the statistical properties of two-dimensional and quasigeostrophic turbulence, by high resolution direct numerical simulations. The first part introduces some fundamental concepts in the understanding of the two turbulent regimes and links these to current research activities. The second part is a collection of the following articles:

Paper 1. A. VALLGREN & E. LINDBORG, 2010

The enstrophy cascade in forced two-dimensional turbulence. $J.\ Fluid\ Mech.$, Article in press.

Paper 2. E. LINDBORG & A. VALLGREN, 2010

Testing Batchelor's similarity hypotheses for decaying two-dimensional turbulence. *Phys. Fluids* **22**, 091704.

Paper 3. A. VALLGREN, 2010

Infrared Reynolds number dependency of the two-dimensional inverse energy cascade. J. Fluid Mech., Accepted.

Paper 4. A. VALLGREN & E. LINDBORG, 2010

Charney isotropy and equipartition in quasi-geostrophic turbulence. J. Fluid Mech. 656, 448.

Paper 5. A. VALLGREN, 2010

Simulations of two-dimensional and quasi-geostrophic turbulence. Internal ${\it Report}.$

Division of work between authors

The research project was initiated by Dr. Erik Lindborg (EL) who has been the main supervisor. Dr. Geert Brethouwer (GB) was co-advisor.

Paper 1

The code was developed and implemented by Andreas Vallgren (AV), in collaboration with EL and GB. Simulations were performed by AV. Most of the paper was written by AV with input from EL. EL wrote the introduction.

Paper 2

The simulations were performed by AV. The paper was written by EL, with input from AV.

Paper 3

The simulations were performed by AV. The paper was written by AV.

Paper 4

The code was developed and implemented by AV, in collaboration with EL. The simulations were performed by AV, who also wrote the paper with input from EL.

Paper 5

The internal report was written by AV.

Parts of this work have been presented at:

Rotating Stratified Turbulence and Turbulence in the Atmosphere and Oceans workshop

December 8-12, 2008, Isaac Newton Institute for Mathematical Sciences, Cambridge, UK.

ECMWF, Reading, UK

January 29, 2010, Invited talk.

Topics in Rotating Stratified Turbulence

August 2-5, 2010, NCAR Geophysical Turbulence Program, Boulder, Colorado, USA.

Euromech Fluid Mechanics Conference 8

September 13-16, 2010, Bad Reichenhall, Germany.



Le seul véritable voyage, le seul bain de Jouvence, ce ne serait pas d'aller vers de nouveaux paysages, mais d'avoir d'autres yeux, de voir l'univers avec les yeux d'un autre, de cent autres, de voir les cent univers que chacun d'eux voit, que chacun d'eux est.

The only true voyage of discovery, the only fountain of eternal youth, would be not to visit strange lands but to possess other eyes, to behold the universe through the eyes of another, of a hundred others, to behold the hundred universes that each of them beholds, that each of them is

Marcel Proust (1871–1922)

vii



Contents

Abstract	iii
Preface	iv
Part I - Introduction	
Chapter 1. Introduction	1
Chapter 2. Strictly two-dimensional turbulence	5
2.1. Introduction	5
2.2. The forward enstrophy cascade	8
2.3. The inverse energy cascade	10
2.4. Decaying two-dimensional turbulence	12
2.5. Coherent structures	13
2.6. β -plane turbulence	15
2.7. Nonuniversal features of the inertial ranges	18
Chapter 3. Quasi-geostrophic turbulence	21
Chapter 4. Numerical method and the codes	24
Chapter 5. Summary of the papers	25
Paper 1	25
Paper 2	25
Paper 3	25
Paper 4	26
Paper 5	26
Chapter 6. Outlook	27
Acknowledgements	28
Appendix A. Derivation of the QG potential	
vorticity equation	29
A.1. Introduction	29
A.2. Scaling the 3D Navier-Stokes equation	29
A.3. The geostrophic approximation	34
A.4. Using static stability to resolve the vertical motion	38

A.5. The quasi-geostrophic potential vorticity equation A.6. Connecting the QGPV equation to Charney's theory A.7. The role of the β -term				
Bibliography				
Part II - Papers				
Paper 1.	The enstrophy cascade in forced two-dimensional turbulence	61		
Paper 2.	Testing Batchelor's similarity hypotheses for decaying two-dimensional turbulence	81		
Paper 3.	Infrared Reynolds number dependency of the two-dimensional inverse energy cascade	91		
Paper 4.	Charney isotropy and equipartition in quasi-geostrophic turbulence	105		
Paper 5.	Simulations of two-dimensional and quasi-geostrophic turbulence	119		

Part I Introduction

CHAPTER 1

Introduction

Welcome to the amazing Flatlands! A very conservative place where only viscosity makes a difference and where new ideas are often abandoned in favour of the original predictions. Two-dimensional turbulence is still, 40 years from when it was more profoundly theoretized, an active research field. Despite the apparent simplicity in dealing with two, rather than three, spatial dimensions, 2D turbulence is possibly richer in its dynamics than 3D turbulence. The reason is found in its conservational properties. Both energy and a multitude of vorticity quantities, called Casimirs, are inviscidly conserved, the latters on a parcel. One such Casimir, enstrophy, defined as $\Omega = \omega^2/2$ where $\omega = \mathbf{e}_z \cdot \nabla \times \mathbf{u}$ is the vorticity and \mathbf{u} is the two-dimensional velocity field, has profound importance in two-dimensional turbulence, as we will see. The conservation properties impose restrictions on the flow evolution and are thus of both mathematical and physical interest. Of most physical relevance, is perhaps the fact that there is no forward energy cascade as in three-dimensional turbulence. Richardson's (1922) view of 3D turbulence was summarized as

Big whorls have little whorls, Which feed on their velocity; And little whorls have lesser whorls, And so on to viscosity.

In two-dimensional turbulence, this picture is reversed, with energy cascading towards larger scales, while enstrophy cascades towards smaller scales. One might then ask why we care about two-dimensional turbulence, seemingly just an academic topic very far from the real world? A few moments thought reveal that it might not be just of academic interest. We may find quasi-two-dimensional flows in a wide variety of situations. One such example is the flow in a fluid film on top of a surface of another fluid or a rigid object. Another example is a rapidly rotating fluid. A third example, which is the main motivation of this thesis, is the approximate 2D nature of tropospheric and oceanic flows (see figure 1.1, illustrating some typical flow structures). This can be understood as a consequence of the small aspect ratio D/L of large scale flow structures, where $D \sim 10$ km is the approximate scale height of the troposphere and $L \sim 1000$ km is the typical length scale of cyclones and anticyclones, advected by a practically horizontal flow. In fact, the motion of

1

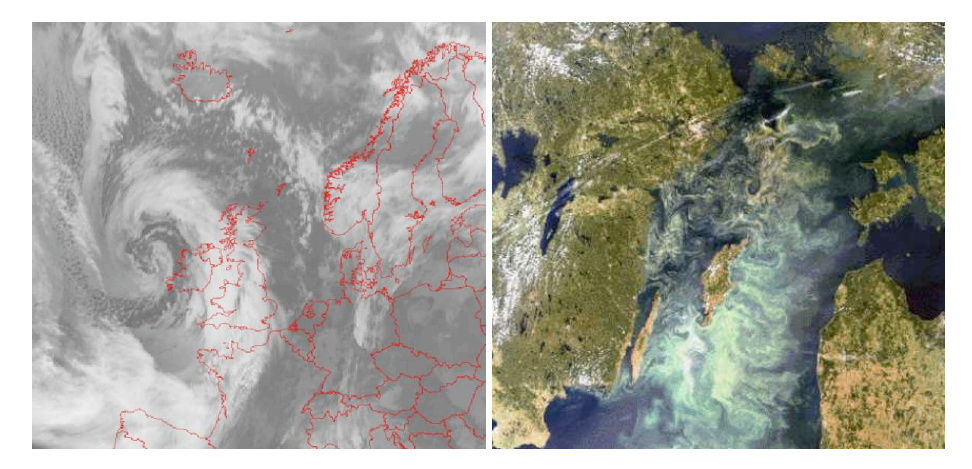


FIGURE 1.1. Examples of quasi-2D flow regimes. Left: Infrared satellite image from March 10, 2008, showing a mature cyclone west of the British Isles. Right: RGB satellite image showing an algal bloom event in the Baltic Sea, acting as a passive tracer in the flow field near the sea surface. From SMHI.

tropical cyclones have been successfully predicted by 2D vortex models (Tabeling 2002). The question is whether the atmospheric (kinetic) energy spectrum can be explained by two-dimensional turbulence. Nastrom & Gage (1985) and Gage & Nastrom (1986) presented observational data on the wave number energy spectrum, showing a k^{-3} kinetic energy spectrum at large scales and a $k^{-5/3}$ -spectrum at scales smaller than about 500 km (see figure 1.2), where k is the wave number. There have been numerous attempts to explain these observations in terms of 2D turbulence over the years, e.g., Lilly (1983), Smith & Yakhot (1994) and Tung & Orlando (2003). Lindborg (1999; 2006) argued that the k^{-3} -range can be explained in terms of a 2D enstrophy inertial range whereas the $k^{-5/3}$ -range should most likely not be interpreted as a result of 2D turbulent interactions. Thus, although there is much evidence for a 2D enstrophy cascade range at large scales, the dynamic origin of the $k^{-5/3}$ -range at high wave numbers is still debated. There are namely two possible candidates for such a range; a forward cascade of stratified 3D turbulent energy (e.g., Lindborg 2006) or an inverse cascade of 2D energy (e.g., Lilly 1983; Smith 2004). The former depends on energy being fed from large-scale baroclinic motions and the latter from convective sources such as thunderstorms. Another suggestion for the observed $k^{-5/3}$ -range is surface-quasigeostrophy (Tulloch & Smith 2009). To settle this question, one needs to increase the complexity in the modeling by allowing for rotation and stratification, which are two important features of tropospheric flow. Charney (1971) derived a theory of what is called quasi-geostrophic turbulence. This turbulent regime takes into account the effect of background rotation and a stable stratification, and describes the flow

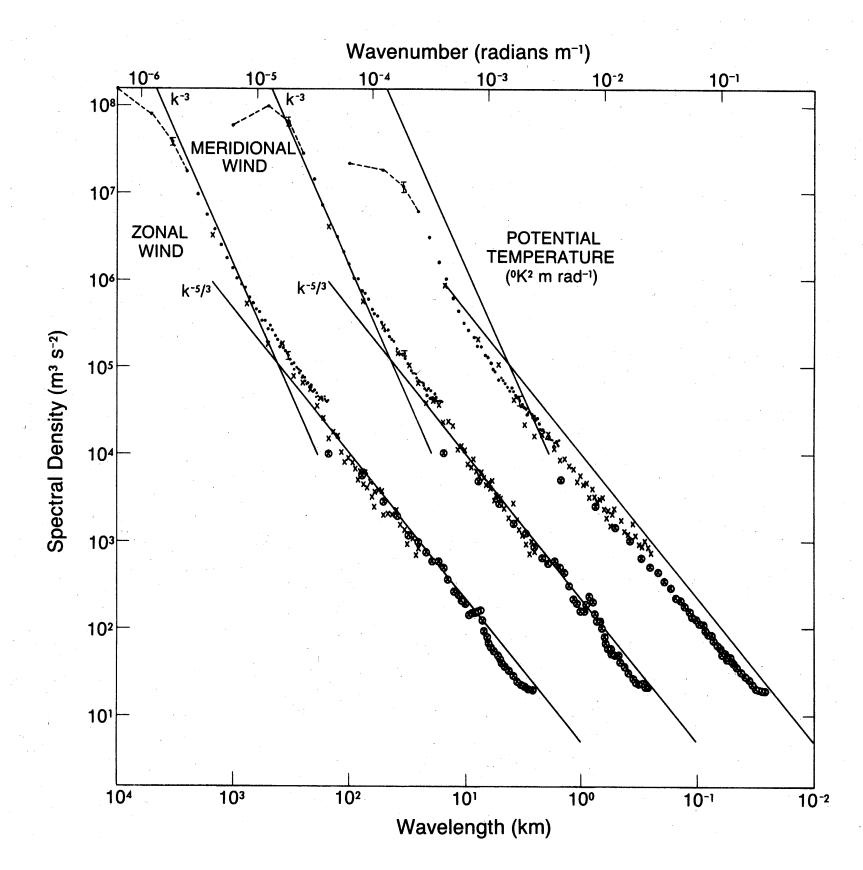


FIGURE 1.2. Observed kinetic energy spectrum divided into zonal and meridional components and potential energy spectrum in terms of the potential temperature, clearly indicating the existence of two spectral ranges. From Nastrom & Gage (1985).

dynamics at relatively large, synoptic, scales. A key point in Charney's theory was the introduction of a stretched coordinate in the vertical, $\zeta = (N/f)z$, where N is the Brunt-Väisälä frequency which is a measure of the stratification and f is the Coriolis parameter which is a measure of the rotation rate. By performing this transformation, Charney predicted a clear analogy with two-dimensional turbulence, in terms of cascade directions and approximately isotropic energy spectra. This thesis explores the statistical characteristics of pure two-dimensional and quasi-geostrophic turbulence in order to approach the subtle question about the origins of the atmospheric energy spectrum. This is accomplished by the development of two codes by which a number of direct numerical simulations have been carried out for these two flow regimes. Not only is the nature of large-scale atmospheric turbulence interesting in its own

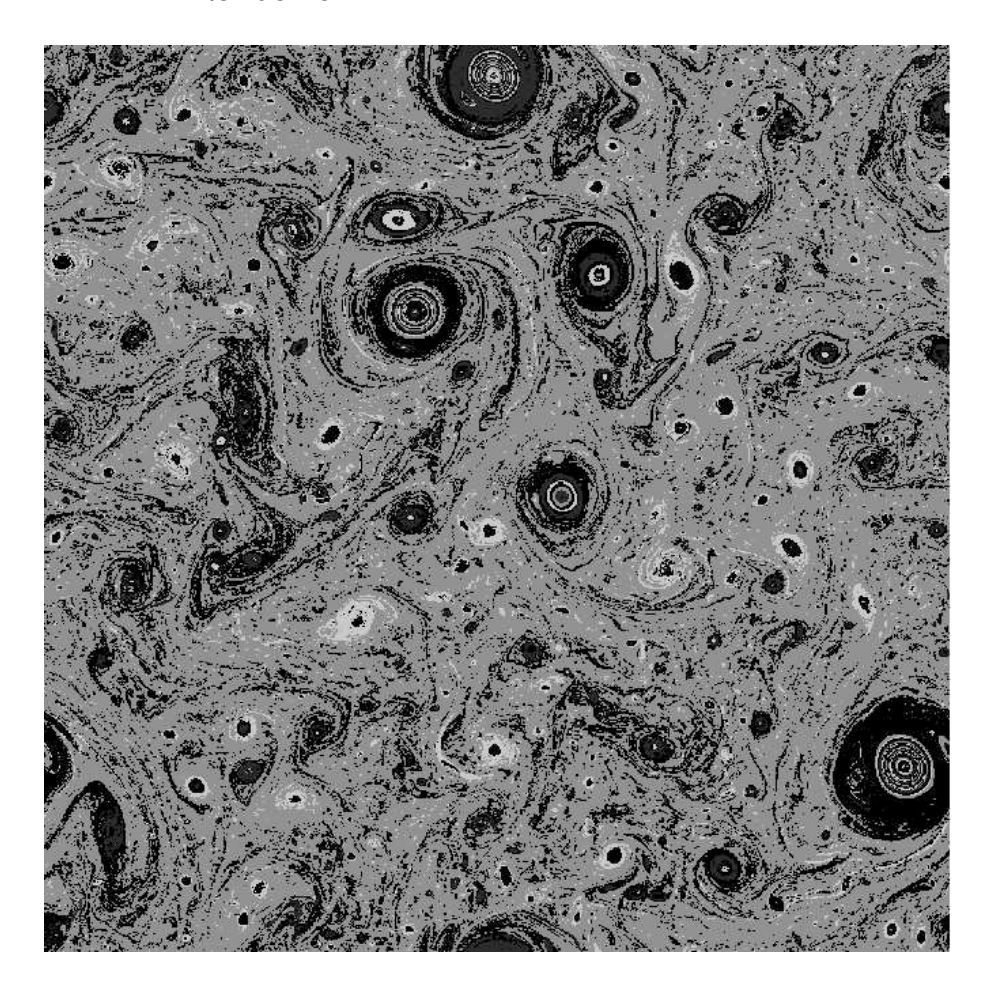


FIGURE 1.3. An artist's view of two-dimensional turbulence? The physics behind two-dimensional turbulence may result in aesthetically appealing features meanwhile important dynamical mechanisms are revealed. There is also a deeper connection to the nature of large-scale atmospheric and oceanic flows.

right, but the outcomes of these studies are also of interest for the development of operational forecast and climate models. The next sections will describe the statistical characteristics of two-dimensional and quasi-geostrophic turbulence in more detail, while figure 1.3 gives a visual interpretation of the phenomena to be explored. For a more thorough review of two-dimensional turbulence, the reader is referred to Tabeling (2002) and Danilov & Gurarie (2000). The latter authors also cover quasi-2D turbulence including quasi-geostrophic turbulence. A more recent review on two-dimensional turbulence subject to bounded domains is provided by Clercx & van Heijst (2009).

CHAPTER 2

Strictly two-dimensional turbulence

2.1. Introduction

Richardson's view of the turbulent cascade of energy cannot be valid in two dimensions. The physical constraints imposed on a two-dimensional flow prevent a dominant forward energy cascade. The constraints follow from inviscid conservation of both energy and enstrophy, which can be realized by deriving the energy and enstrophy equations resulting from multiplying the 2D Navier-Stokes equation by ${\bf u}$ and the vorticity equation by ω , respectively. The incompressible Navier-Stokes equation in its vorticity formulation is given by

$$\frac{\partial \omega}{\partial t} + (\boldsymbol{u} \cdot \nabla)\omega = \nu \nabla^2 \omega, \tag{2.1}$$

where ν is the kinematic viscosity. One way to picture the role of the inviscid ($\nu = 0$) conservation properties is to consider the temporal evolution of the energy and enstrophy centroid wave numbers, respectively, following Vallis (2006). Noting that the mean energy and enstrophy can be written as

$$\bar{E} = \frac{1}{2} \int \left(u^2 + v^2 \right) dA = \frac{1}{2} \int \left[\left(\frac{\partial \psi}{\partial y} \right)^2 + \left(\frac{\partial \psi}{\partial x} \right)^2 \right] dA, \tag{2.2}$$

$$\bar{\Omega} = \frac{1}{2} \int \omega^2 dA = \frac{1}{2} \int \left(\nabla^2 \psi \right)^2 dA, \qquad (2.3)$$

where $\omega = \mathbf{e}_z \cdot \nabla \times \mathbf{u}$ is the vorticity and the stream function ψ is defined so that $u = -\partial \psi/\partial y$, $v = \partial \psi/\partial x$ and $\omega = \nabla^2 \psi$, and transforming into spectral space, we obtain

$$\bar{E} = \int E(k)dk = \frac{1}{2} \int (\widehat{u}\widehat{u}^* + \widehat{v}\widehat{v}^*)dk = \frac{1}{2} \int k^2 \widehat{\psi}\widehat{\psi}^*dk, \qquad (2.4)$$

$$\bar{\Omega} = \int \Omega(k)dk = \frac{1}{2} \int \widehat{\omega}\widehat{\omega}^* dk = \frac{1}{2} \int k^4 \widehat{\psi}\widehat{\psi}^* dk = \int k^2 E(k)dk, \qquad (2.5)$$

where E(k) and $\Omega(k)$ are the energy and enstrophy wave number spectra. We now define the energy centroid wave number as

$$k_E = \frac{\int kE(k)dk}{\int E(k)dk},\tag{2.6}$$

and introduce the quantity

$$I = \int (k - k_E)^2 E(k) dk = \int k^2 E(k) dk - k_E^2 \int E(k) dk, \qquad (2.7)$$

which upon temporal differentiation gives a measure of the spreading of the energy distribution. To obtain the last equality in (2.7), the definition of k_E (2.6) has been used. If all energy is initially centred at k_E , dI/dt should be larger than zero. Since both energy and enstrophy are inviscibly conserved, it follows that

$$\frac{dk_E}{dt} = -\frac{1}{2k_E\bar{E}}\frac{dI}{dt} < 0, (2.8)$$

(2.9)

which is consistent with an inverse energy cascade, i.e., a transfer of energy towards larger scales. Similarly, if we define an enstrophy centroid wave number k_{Ω} as

$$k_{\Omega} = \frac{\int \Omega(k)dk}{\int k^{-1}\Omega(k)dk},$$
(2.10)

and introduce

$$J = \int (k^{-1} - k_{\Omega}^{-1})^2 \Omega(k) dk = \int E(k) dk - k_{\Omega}^{-2} \int \Omega(k) dk, \qquad (2.11)$$

a little manipulation yields

$$\frac{dk_{\Omega}}{dt} = \frac{k_{\Omega}^3}{2\bar{\Omega}} \frac{dJ}{dt} > 0. \tag{2.12}$$

Thus, the enstrophy centroid wave number (in which all enstrophy is initially located) moves towards higher wave numbers (smaller scales) with time, which can be interpreted as a forward cascade of enstrophy. These are heuristic arguments but nevertheless show the general tendency of the cascade directions. Note that these arguments do not forbid energy/enstrophy to be transferred to smaller/larger scales, they just tell us that more energy/enstrophy propagates towards larger/smaller scales than in the opposite direction. As could be understood from the preceeding discussion, the fluxes of energy and enstrophy are an integral part in the description of flow characteristics. We thus start by noting that

$$\frac{\partial E(k)}{\partial t} = T(k) + D(k) + F(k), \tag{2.13}$$

where

$$T(k) = \frac{1}{2\pi} k_i \int_0^{2\pi} Im \left[\widehat{u_i u_j}(\mathbf{k}) \widehat{u_j}^*(\mathbf{k}) \right] d\theta_k$$
 (2.14)

is the (nonlinear) transfer of energy associated with the scalar wave number k, following an integration in wave number space of $\mathbf{k} = k[\cos(\theta_k)\mathbf{e}_x + \sin(\theta_k)\mathbf{e}_y]$ over an azimuthal angle θ_k , and * denotes the complex conjugate. D(k) is the dissipation, which in the case of Navier-Stokes viscosity is given by

$$D(k) = -2\nu k^2 E(k) + D_{\alpha}(k), \tag{2.15}$$

where $D_{\alpha}(k)$ is a large-scale sink such as Ekman drag or hypodiffusion. The term F(k) corresponds to any particular forcing of wave mode k. The energy flux is thence given by

$$\Pi_E(k) = -\int_0^k T(k')dk',$$
(2.16)

and the enstrophy flux follows accordingly (cf eq. 2.5) as

$$\Pi_{\Omega}(k) = -\int_{0}^{k} k'^{2} T(k') dk'. \tag{2.17}$$

Our next step is to elaborate on the existence of a double cascade scenario and inertial ranges in two-dimensional turbulence. Let us consider a case in which we feed a turbulent system with energy at a scale k_f . Given that the general picture of the cascade directions holds, as reflected by the time evolution of the centroid wave numbers, we would expect energy to propagate upscale and enstrophy to propagate downscale. If there is no large-scale drag imposed and we consider an infinitely large domain, we would expect an undisturbed energy cascade towards larger scales. Simultaneously, we would expect an enstrophy cascade towards smaller scales, where enstrophy is ultimately removed by smallscale viscous dissipation. Given a large enough Reynolds number so that $k_f \ll$ k_{max} , it is reasonable to expect that there would be a region, $k_f < k < k_{max}$, practically undisturbed by viscous dissipation. Assume that we feed the system with energy at a rate ϵ and enstrophy at a rate η (the two are related by $\epsilon = \eta/k_f^2$). In the energy cascade range, the only parameters of practical importance would be the energy density E(k), the energy injection rate ϵ and wave number k. Accordingly, we let $E(k) \sim \epsilon^a k^b$. Dimensional reasoning gives that a = 2/3 and b = -5/3 so that $E(k) \sim \epsilon^{2/3} k^{-5/3}$. A similar argument gives that $E(k) \sim \eta^{2/3} k^{-3}$ in the forward enstrophy cascade range. These predictions were introduced by Kraichnan (1967) and Leith (1968) and are illustrated in figure 2.1. Thus, for the inverse energy cascade range,

$$E(k) = \mathcal{K}\epsilon^{2/3}k^{-5/3},\tag{2.18}$$

and for the enstrophy cascade range;

$$E(k) = C\eta^{2/3}k^{-3},$$
 (2.19)

where we refer to \mathcal{C} as the Kraichnan constant in forced two-dimensional turbulence and the Batchelor-Kraichnan constant in decaying two-dimensional turbulence (Batchelor 1969). One major assumption that these predictions rely on is the locality of the cascades, meaning that it is assumed that there is no interaction between widely separated scales. In particular, in each of the inertial ranges, there can be no strong influence from scales outside of these (Vallis 2006). It can be noted, however, that Kraichnan (1967 & 1971) was uncertain about the validity of a locality assumption in two-dimensional turbulence as compared to the three-dimensional analogue. Already in 1967, Kraichnan hypothesized that a logarithmic correction should manifest in the k^{-3} enstrophy cascade range, although he did not provide any exact details on its form.

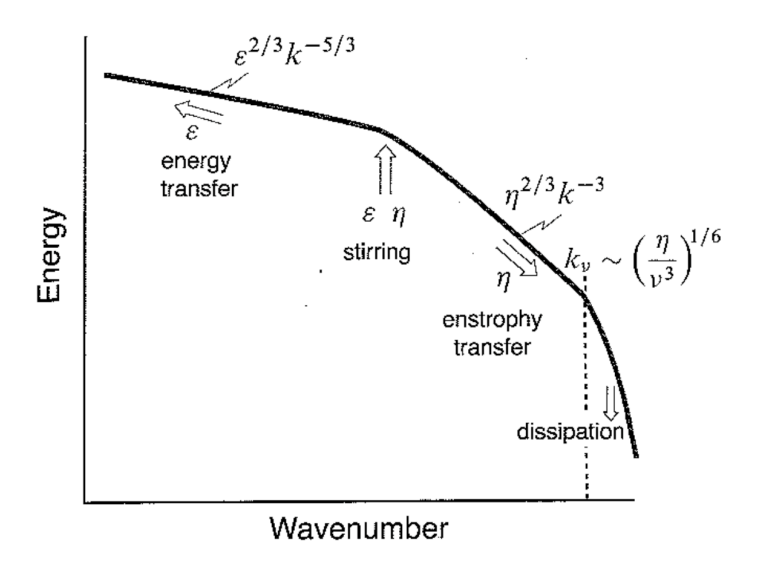


FIGURE 2.1. Qualitative picture of the double cascade of forced two-dimensional turbulence. From Vallis (2006).

In a follow-up paper, Kraichnan (1971), provided a complimentary theoretical prediction, namely

$$E(k) = C' \eta_{\omega}^{2/3} k^{-3} \left[\ln \left(\frac{k}{k_1} \right) \right]^{-1/3},$$
 (2.20)

where \mathcal{C}' is a constant of order unity, which Kraichnan estimated to 2.626 based on a turbulence test-field model and k_1 marks the lowest wavenumber of the inertial range. The correction allows for a k-independent \mathcal{C}' and a constant enstrophy flux range.

2.2. The forward enstrophy cascade

In this section we review the enstrophy cascade in forced two-dimensional turbulence. The cascade theory of Kraichnan (1967) has been tested numerically in a large number of studies. At the time of the early theoretical advances, the computational resources were very limited, but attempts were made to simulate the two-dimensional Navier-Stokes equation. However, the limited resolution available at this time was only enough to indicate a qualitative statistical picture of low Reynolds number 2D turbulence. During the 1980's and 1990's, the computational resources allowed for more resolved and more accurate numerical simulations. The results from these experiments indicated that the k^{-3} or possibly the logarithmically corrected spectrum, was not as robust as anticipated, with reports on steeper energy spectrum (e.g., Legras et al. 1988; Gilbert 1988;

Maltrud & Vallis 1991 and Kaneda & Ishihara 2001). The presence of vortices was believed to distort the spectral shape of the energy spectrum in the enstrophy inertial range. However, with ever-increasing computational resources, the results once again started to point towards the early theoretical predictions by Kraichnan-Leith (e.g., Lindborg & Alvelius 2000; Boffetta 2007 and Bracco & McWilliams 2010). The logarithmically corrected enstrophy spectrum has been numerically obtained by, e.g., Pasquero & Falkovich 2002. Most of these studies have included a large-scale friction (also referred to as drag or hypodiffusion) to prevent energy from growing at the largest scales and drive the turbulence into a stationary state where energy is dissipated at large scales at the same rate at which it is injected. If the turbulence is forced at a very small wave number, corresponding to the scale of the computational domain, and no large scale drag is introduced, energy will pile up in the smallest wave numbers and there is a clear risk that a state soon develops which is very different from the double cascade scenario. If the turbulence is forced at a considerably larger wave number, it will become extremely demanding to resolve a sufficiently large span of scales to obtain a broad enstrophy cascade range. Thus, no serious attempt was made to test the perhaps strongest prediction of Kraichnan's theory - the existence of a stationary enstrophy cascade in the absence of large scale drag and in the presence of a constant energy growth. However, we have now performed such simulations. A series of extremely high resolution simulations, presented in Paper 1, suggests that the enstrophy cascade may indeed be more robust than currently believed. In the absence of a large scale drag, we have obtained results that confirm Kraichnan's original prediction (1967) with a clean k^{-3} energy spectrum in the enstrophy cascade range, without the logarithmic correction that Kraichnan proposed in his follow-up paper (1971). Figure 2.2 illustrates the real vorticity field in a simulation forced at large scales. In particular, note the dominance of vorticity filaments, indicative of the forward enstrophy cascade. This cascade dominates the dynamics at several wave number decades, as shown in figure 2.3. However, the universality might fail with respect to the constant C, which has been found to vary slightly in our simulations, as a consequence of large-scale dissipation anomalies in association with coherent vortices.

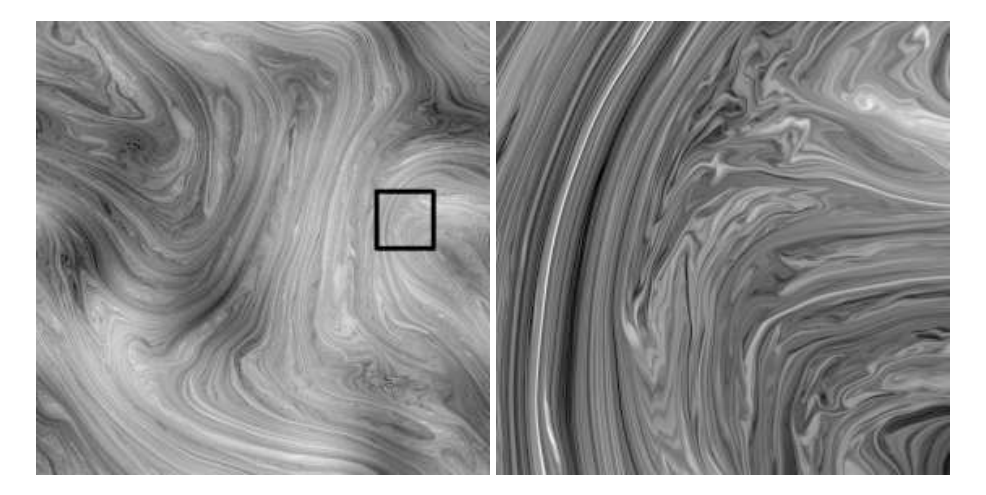


FIGURE 2.2. Vorticity field and zoom in from a simulation forced at large scales, showing the dominance of vorticity filaments, resulting from a forward enstrophy cascade.

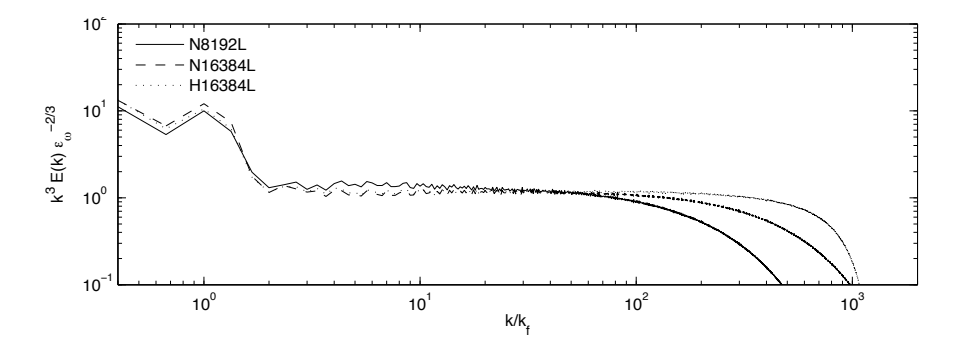


FIGURE 2.3. Compensated energy spectra, $k^3 E(k) \epsilon_{\omega}^{-2/3}$, from a set of very high resolution simulations of forced two-dimensional turbulence.

2.3. The inverse energy cascade

A stationary inverse energy cascade range can only be obtained in the presence of a large scale drag, since energy would otherwise cascade indefinitely towards larger scales. In reality, there is always a physical limit on how far the cascade can reach, namely the domain size. As energy reaches the smallest wave number, it will continuously pile up at this wave number, forming a condensate. Such a condensate will bring the system away from the double cascade scenario by Kraichnan-Leith (e.g., Smith & Yakhot 1994). In order to generate a double cascade with two wide inertial ranges, very high resolution

simulations are required. Boffetta (2007) and Boffetta & Musacchio (2010) performed such simulations, showing a nearly perfect $k^{-5/3}$ inverse cascade range in the presence of a linear drag, while obtaining an enstrophy inertial range a little steeper than k^{-3} . A linear drag is often introduced as a large-scale energy dissipation mechanism, found in real systems such as the atmosphere (Ekman friction) and in physical experiments. Boffetta (2007) investigated the fluxes of energy and enstrophy in physical space and found that there is a very small correlation between these fluxes. This suggests that it should be possible to generate an energy cascade range without the presence of an enstrophy cascade range, which was also proposed by Tran & Bowman (2004). Therefore, it seems plausible that simulations with forcing at scales near the small-scale dissipation range will give the classical $k^{-5/3}$ -spectrum. However, this suggestion can be questioned. Starting with Borue (1994), it was found that the implementation of a large-scale hypodiffusion steepens the energy spectrum considerably to almost a k^{-3} -spectrum. The possible reason was found in the existence of vortices over all scales, whereas Boffetta et al. (2000) explained it in terms of a bottleneck effect as in three-dimensional turbulence (Falkovich 1994; Bos & Bertoglio 2009). However, Smith & Yakhot (1994) found that the $k^{-5/3}$ -spectrum steepened to an exponent $\lesssim -2$ when both of the cascades are resolved, as a consequence of vortex generation in the enstrophy cascade range. This result was later confirmed by Scott (2007), who used high resolution simulation to provide estimates on when this steepening occurs. To summarize, the issue seems rather involved, and there is no clear evidence for a universal energy inertial range controlled by local interactions, as highlighted by Maltrud & Vallis (1993) and Danilov & Gurarie (2001a, 2001b). As a response to these differing results, we have performed a set of high resolution simulations with and without a large scale linear drag of varying strength and with a variable forcing wave number. It has been found that the form of the energy spectrum is sensitive to the strength of the large scale drag. In paper 3 we introduce an infrared Reynolds number $Re_{\alpha} = k_f/k_{\alpha}$, where k_f is the forcing wave number and k_{α} is a frictional wave number, and demonstrate that the $k^{-5/3}$ energy spectrum steepens to k^{-2} or steeper at high Re_{α} as a consequence of vortex formation in the inverse cascade range. It is also found that the inverse cascade is dominated by nonlocal interactions, as described in more detail in section 2.7. To close this section, it can be noted that the physical mechanisms behind the inverse energy cascade are still debated. The explanations range from vortex merging, as in decaying turbulence, (e.g. McWilliams 1990), like-sign vortex clustering (e.g. Boffetta et al. 2000) and skew-Newtonian stress (see Chen et al. 2006, who address the question about physical mechanisms but lack the locality discussion). A tentative reason behind the formation of vortices is perhaps associated with the observations by Elhmaidi et al. (2005). They suggested that the presence of a linear drag induces filament instabilities that may lead to the formation of coherent vortices.

2.4. Decaying two-dimensional turbulence

Decaying two-dimensional turbulence describes the evolution of a flow field in the absence of forcing and without any large scale dissipation, principally conserving energy at high Reynolds number. In that sense, decaying 2D turbulence might be considered as the purest kind of turbulence we can study. However, the initial conditions may differ considerably, although this should not cause any different results at small scales, if the evolution is to be universal, as predicted by Kraichnan, Batchelor and Leith. Therefore, it would seem natural that this case should be subject to less dispute. However, this is not the case. In fact, decaying 2D turbulence has been subject to renewed interest. As an initial flow field is released to decay freely, we could expect energy to cascade towards larger scales, where it is unaffected by small-scale viscosity, and so conserving energy, whereas the enstrophy would cascade towards smaller scales where it is dissipated. The question is how the energy spectrum evolves under these circumstances. According to Batchelor (1969), the enstrophy dissipation rate χ should stay finite in the limit $\nu \to 0$ and the inertial range enstrophy spectrum should be given by

$$\Omega(k) = \mathcal{C}\chi^{2/3}k^{-1},\tag{2.21}$$

where \mathcal{C} is a universal constant. However, this theoretical prediction has been questioned. According to Tran & Dritschel (2006), the enstrophy dissipation vanishes in the limit $\nu \to 0$ and in a follow-up paper, Dritschel et al. (2007) suggested that the enstrophy spectrum should instead scale according to

$$\Omega(k) = \Omega k^{-1} (\ln Re)^{-1},$$
(2.22)

where $Re \equiv \Omega/\nu k_0^2$. They also argued that the inertial range should contain an increasing portion of the total enstrophy with increasing Reynolds number. Batchelor (1969) was, however, aware of the potential inconsistency in the assumption of a strictly finite χ in the inviscid limit. He noted that, with an enstrophy spectrum given by (2.21), the total mean square vorticity diverges as $\chi^{2/3} ln\left(Re\right)$ as $\nu \to 0$, which would allow the total enstrophy to be larger than the initial enstrophy, which is impossible. He remedied this by conjecturing that χ becomes so small at high Re that $\chi^{2/3}ln(Re) \leq \Omega_0$. Thus, it seems that he gave up the assumption of a strictly finite χ in the inviscid limit. Thus, even if $\chi \to 0$ as $Re \to \infty$, Batchelor assumed that χ decreases in such a way that the prediction (2.21) still holds. This has in fact been corroborated by our simulations in paper 2, which were performed in order to test Batchelor's hypotheses, with the largest resolutions presented so far in the literature. Although there is an implicit Reynolds number dependency, the effect of this is so small that it is not visible in our results (see figure 2.5, top). The figure demonstrates the compensated (following the prediction by Batchelor and Dritschel et al.) enstrophy spectra $\Phi(k)$ from three simulations with different initial conditions, taken at three instances in time. The Dritschel et al. prediction gives rather large departures from a universal collapse in the equilibrium range, as seen in figure 2.5, bottom. This despite the fact

that $\chi^{2/3} << \Omega / ln \, Re$ in our simulations, which is consistent with $\chi \to 0$ as $Re \to \infty$. In addition, the prediction of Dritschel et al. that the inertial range should contain an increasing portion of the total enstrophy with Re did not find any support in our simulations. As a matter of fact, as t >> 0, an ever-increasing portion of the total enstrophy was contained at scales larger than the inertial range scales meaning that the enstrophy content in the inertial range was even more reduced than could be anticipated. This was due to the presence of strong and relatively stable coherent vortices.

Our simulations also show that the Batchelor-Kraichnan constant \mathcal{C} is of order unity, but varies slightly, as a consequence of a high degree of intermittency in the enstrophy dissipation. The slight variation of the constant can be explained following an argument by Landau (Landau & Lifshitz 1987). In essence, we reproduced Batchelor's result, with a k^{-1} enstrophy spectrum in all our simulations, despite very different initial conditions, which are visible also at later times (see figure 2.4). It is noteworthy that the steeper spectra obtained by earlier investigators (e.g., McWilliams 1984 and Bartello & Warn 1996), might be an artefact of a low Reynolds number, since the width of the enstrophy inertial range decreases slowly with time as the dissipation wave number $k_d \sim \chi^{1/6} \nu_{\omega}^{-1/2}$, and χ decreases with time. We have also found that power law exponents of decay rates of quantities such as the enstrophy and hence enstrophy dissipation are dependent on the initial conditions. This is consistent with the observations by van Bokhoven et al. (2007).

2.5. Coherent structures

We have performed a number of simulations revealing the existence of strong and long-lived vortices which we refer to as coherent structures. They are easy to distinguish by the human eye as they stand out as ordered structures in a chaotic sea of filamentary vorticity debris (see figure 2.4 and close-up of an individual vortex in 2.6). They are also belived to cause departures from universal scaling laws in two-dimensional turbulence. McWilliams (1984, 1990) found early evidence of stuctures containing a substantial fraction of vorticity of two-dimensional flows, with lifetimes far exceeding the characteristic time for nonlinear interactions. He found that vortices spontaneously develop if the forcing and friction is relatively weak and the Reynolds number is sufficiently large. These vortices are approximately axisymmetric and are stable to perturbations from the quiescent surroundings but not to encounters by other strong vortices. Such encounters can result in like-sign vortex mergers. McWilliams (1990) noted that the lock-up of vorticity inside coherent vortices effectively reduces cascade rates of both enstrophy and energy. By introducing a vortexcensus algorithm, he enabled detailed studies of their properties and found a general trend of the "survival of the fittest". It has also been found that vorticity extremum is quasi-conserved (Carnevale et al. 1991, Maltrud & Vallis 1993 and Scott 2007), resulting in a small inverse enstrophy flux. Dritschel (1995) contributed with a detailed study of vortex interactions and showed that these

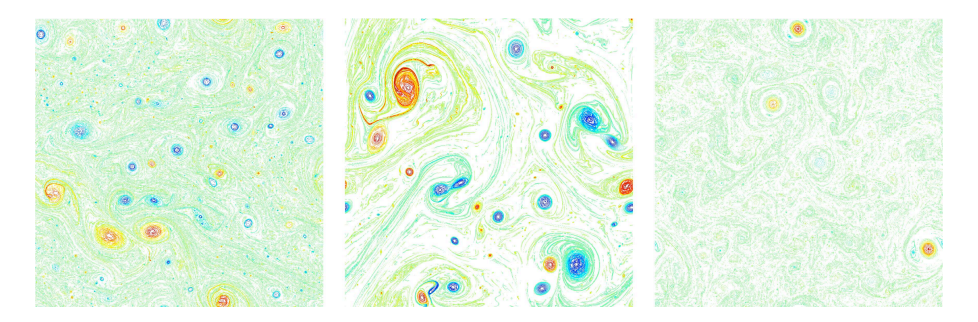


FIGURE 2.4. Snapshots of the "final" states from three simulations of decaying two-dimensional turbulence with various initial conditions. Red colour corresponds to positive vorticity and blue colour to negative vorticity.

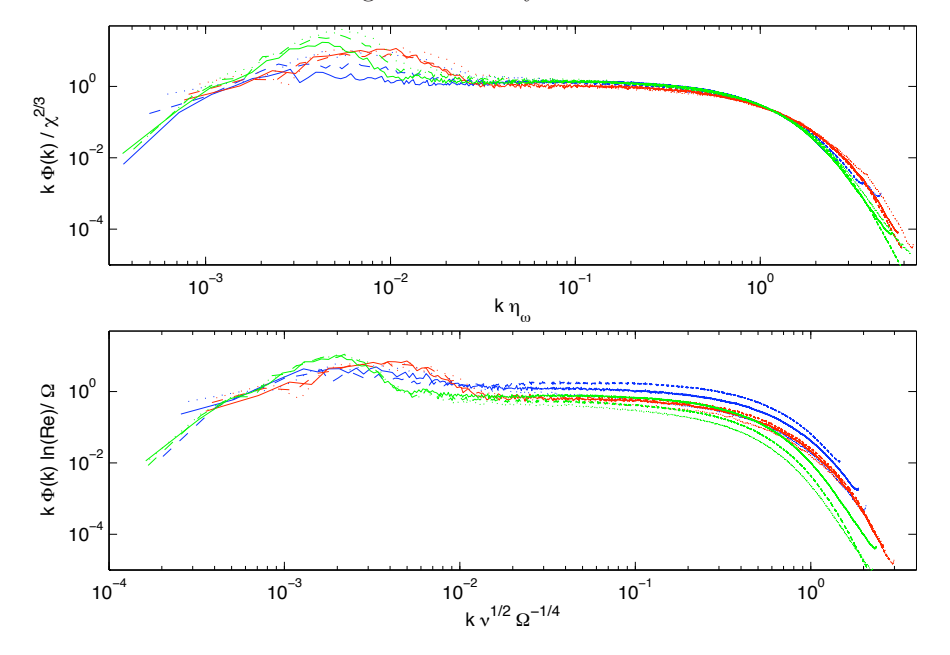


FIGURE 2.5. Compensated enstrophy spectra (as predicted by Batchelor (top) and Dritschel et al.; bottom) from three simulations (red, blue and green) of decaying two-dimensional turbulence, taken at three instances in time (solid, dashed and dotted). The abscissas are nondimensional wavenumbers, where $\eta_{\omega} = \nu^{1/2} \chi^{-1/6}$.

are relatively short inelastic interactions resulting in two or three new coherent vortices, thus questioning the picture of the inverse energy cascade as a series of merging events resulting in ever-growing vortices, as suggested by, e.g.,

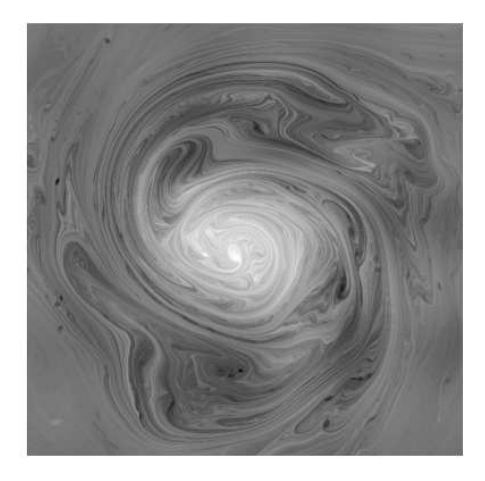


FIGURE 2.6. Close-up of a single vortex revealing its finescale structure.

Borue (1994), in forced two-dimensional turbulence. In decaying turbulence, it is more evident that large-scale structures form as a result of vortex mergers, finally resulting in two opposite-sign vortices (Tabeling, 2002). An interesting question is whether any universal theory can account for coherent vortices. Carnevale et al. (1991) suggested such a theory for vortex circulation, radius, mean enstrophy and kurtosis, but there are ample examples of deviations from such a governing theory (Tabeling, 2002).

2.6. β -plane turbulence

To accommodate for a differential rotation system, a β -term can be added to the 2D Navier-Stokes equation,

$$\frac{\partial \omega}{\partial t} + (\boldsymbol{u} \cdot \nabla)\omega = -\nu \nabla^2 \omega - \beta v. \tag{2.23}$$

The presence of the β -term can be motivated by the following argument. We consider a rotating sphere such as illustrated in figure 2.7, and note that the Coriolis force $2\Omega \times \mathbf{u}$ can be rewritten by defining

$$f \equiv 2\Omega \sin \phi e_z, \tag{2.24}$$

where \mathbf{e}_z is the normal unit vector to a locally Cartesian tangent plane on the sphere. For small variations in the meridional direction

$$f = 2\Omega \sin \phi \simeq 2\Omega \sin \phi_0 + 2\Omega(\phi - \phi_0) \cos \phi_0, \tag{2.25}$$

and we approximate the Coriolis parameter to vary linearly on the tangent plane as

$$f = f_0 + \beta y, \tag{2.26}$$

where

$$f_0 = 2\Omega \sin \phi_0, \tag{2.27}$$

and y is the meridional coordinate on the tangent plane. Thus,

$$\beta = \frac{df}{dy} = \frac{2\Omega\cos\phi_0}{a},\tag{2.28}$$

where a is the radius of the Earth. Equation (2.23), known as the β -plane approximation, describes the motions on a tangent plane of a rotating sphere, provided that the flow is spatially limited so that the geometric effects of sphericity are negligible. It allows for the use of a local Cartesian representation of the Navier-Stokes equation, while still capturing the important dynamical effects stemming from differential rotation.

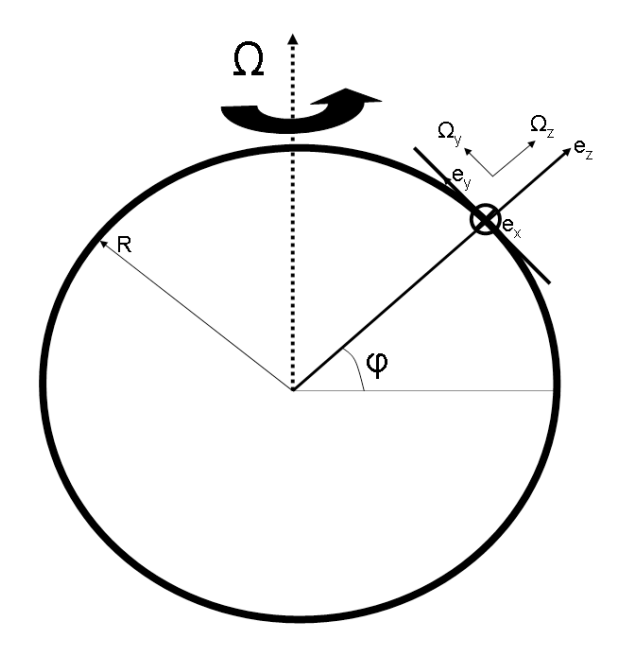


FIGURE 2.7. Tangent plane approximation to the quasispherical Earth. The rotation vector components in the plane are shown as well as the direction of the unit vectors.

We may now ask what the dynamical consequences are of the β -term. Rhines (1975) investigated this matter and showed that turbulent energy is dispersed into waves at length scales larger than approximately

$$l_{\beta} = \sqrt{\frac{2\sqrt{\overline{E}}}{\beta}},\tag{2.29}$$

where \overline{E} is the r.m.s. energy of the flow. There exists a number of definitions of this *arrest* scale, which do not differ too much. Thus, the inverse energy

cascade continues up to a scale l_{β} , from which no upscale energy cascade is possible. Instead, the transition to wave propagation (Rossby waves) is overtaken by a flow characterized by steady alternating zonal jets. This picture is helpful in explaining the characteristic size of eddies in the Earth's atmosphere, and the prevalence of zonal flows. The waves are referred to as Rossby waves, and their dispersion relation can be obtained by linearizing (2.23) upon a basic state. Rossby waves are an important ingredient in atmospheric dynamics, with large effects on both daily weather and regional climate. Many numerical experiments over the years have to a large degree verified Rhines' prediction. Maltrud & Vallis (1991) found that the β -effect tend to destroy coherent vortices at large scales but that the resulting anisotropy at scales larger than l_{β} does not influence the inertial range characteristics at smaller scales. Later studies have concerned the statistical characteristics of the resulting zonal jets (e.g., Vallis & Maltrud 1993; Manfroi & Young 1998; Danilov & Gurarie 2004). It is noteworthy that attempts have been made to explain the atmospheric flow structure on Jupiter, with its zonal jets and superstationary vortices, in terms of two-dimensional or quasi-geostrophic turbulence with a β -effect (e.g., Kukharkin & Orszag 1996; Smith 2004). An example of a simulation with a β effect is shown in figure 2.8 (left), where the anisotropy at large scales is clearly visible. Figure 2.8 (right) also shows a satellite image of Jupiter, with the characteristic zonal flow and the famous red spot visible as a coherent vortex in the southern hemisphere.

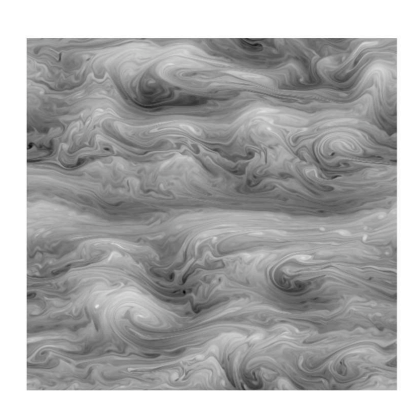




FIGURE 2.8. Left: vorticity snapshot from a simulation with moderate β . Right: satellite image of Jupiter's atmosphere (from NOAA).

2.7. Nonuniversal features of the inertial ranges

Numerous high-resolution numerical simulations have revealed the existence of departures from the classical theory of the two-dimensional inertial ranges. Vortices are not covered by the classical theory, but have been shown to be abundant in our simulations. Traditionally, these have been suggested to be the origin of the steepening of the energy spectrum in the enstrophy cascade range, as observed in many early numerical experiments. However, a different view point will be advanced here, where the scaling of the energy spectrum in the enstrophy cascade range is more or less unaffacted by the presence of vortices. Instead, it is the universality of the Kraichnan-Batchelor constant that is questioned. As found in simulations of both forced and decaying two-dimensional turbulence, the Batchelor-Kraichnan constant is not a perfect constant, but varies slightly between different realisations of numerical experiments. The origin of these variations is most probably a consequence of intermittency in the enstrophy dissipation, being it temporal or spatial. This observation, originally concerning temporal variations, has been known as Landau's objection to the Kolmogorov 1941 theory for three-dimensional turbulence, and was raised already in 1942 (Frisch 1995). Landau (Landau & Lifshitz 1987) concluded that there is a temporal (and spatial, see Kraichnan 1974, Frisch 1991) variance of the dissipation. This variance will differ between different flows. The spatial analogue suggests that the dissipation is intermittent at scales larger than inertial range scales and can therefore not result in a universal averaging of the dissipation. Kraichnan (1974) concluded that the nonuniversality is a result of spatial averaging over the domain scale, which contains patches of enhanced dissipation larger than the inertial scales. Thus, when determining the dissipation rates, it should be taken as an ensemble average over subdomains. In this thesis, it is shown that the Landau argument is perhaps even more important in two-dimensional turbulence than in three-dimensional turbulence, due to the presence of very strong coherent vortices and filamentation in the former. Figure 2.9 shows the probability distribution (left) of χ_i/χ for a set of simulations of freely decaying two-dimensional turbulence, of which one was found to give a different value of \mathcal{C} . Using the notation of Batchelor (1969), χ is here the enstrophy dissipation averaged over the whole flow field (previously denoted by ϵ_{ω}) and χ_i is the enstrophy dissipation averaged over a subdomain whose size is equal to the largest inertial range scale. The simulation with an anomalously low value of \mathcal{C} is characterised by a much broader probability distribution of χ_i , as compared to the other two. As can be understood from figure 2.9 (right), the dissipation rate is enhanced in conjunction with vortices, which consists of spiralling vorticity filaments with steep vorticity gradients.

The inverse energy cascade range has been found to be subject to another, perhaps more fundamental and severe, violation to the basic assumptions, namely, the assumption of spectral locality of the inverse energy cascade. As discussed in section 2.3, numerical experiments have revealed that vortices may develop

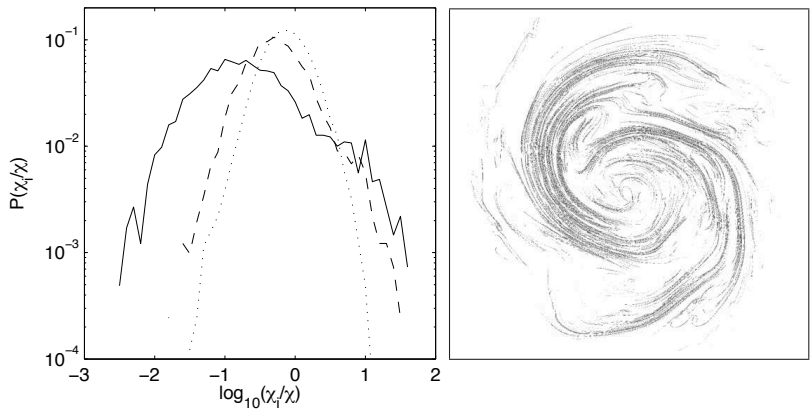


FIGURE 2.9. Left) Probability distribution of χ_i/χ for subdomains compared to the mean dissipation of the whole domain for three simulations of freely decaying two-dimensional turbulence. Right) Snapshot of instantaneous dissipation in one vortex.

also in the inverse cascade range, resulting in a steeper energy spectrum. Starting with Maltrud & Vallis (1993), it was found that nonlocal effects are present to some degree in the inverse cascade range, despite the fact that they obtain energy spectra close to $k^{-5/3}$. Nonlocal effects have subsequently been traced in studies such as Verma et al (2005) and Danilov & Gurarie (2001). By performing the highest resolution simulations of the inverse energy cascade range so far reported, we found that the inverse energy cascade is completely maintained by nonlocal triad interactions, while the local triad interactions give rise to a forward energy cascade. This is a remarkable result since it questions the validity of the basic locality assumption. To investigate the triad interactions, the transfer function

$$T_{\mathbf{kpq}} = k_j \operatorname{Im} \left[\widehat{u}_j(\mathbf{q}) \widehat{u}_i(\mathbf{p}) \widehat{u}_i^*(\mathbf{k}) \right],$$
 (2.30)

is studied. Here, $\mathbf{q} = \mathbf{k} - \mathbf{p}$, the hat represents the Fourier transform and * represents the complex conjugate. After integration over an azimuthal angle in **k**-space, $T_{\mathbf{kpq}}$ can be written as a function T_{kpq} , of the scalar wave numbers k,p and q. In turn, T_{kpq} can be written as a function, T_{kp} , of k and p, after integration over q. The resulting wave number shell energy flux, $\Pi(k) = -\sum_{0}^{k} \sum_{p} T_{kp}$, of one of the simulations with $k_f = 1000$ is presented in figure 2.10. It shows the energy flux partitioned into a local and nonlocal part, respectively, as well as the sum of these two for a range of locality thresholds $(p \land q \in [1/2k, 2k], [1/4k, 4k], [1/5k, 5k]$ and [1/8k, 8k] defining locality). It is clear that the nonlocal part gives rise to a dominating inverse energy flux for $(p \lor q)/k \ni [(1/a), a]$ for a up to 5, whereas the local part gives rise to a weak forward cascade. Thus, there is new evidence for a highly nonlocal energy transfer, consistent with the findings by Maltrud & Vallis (1993). This

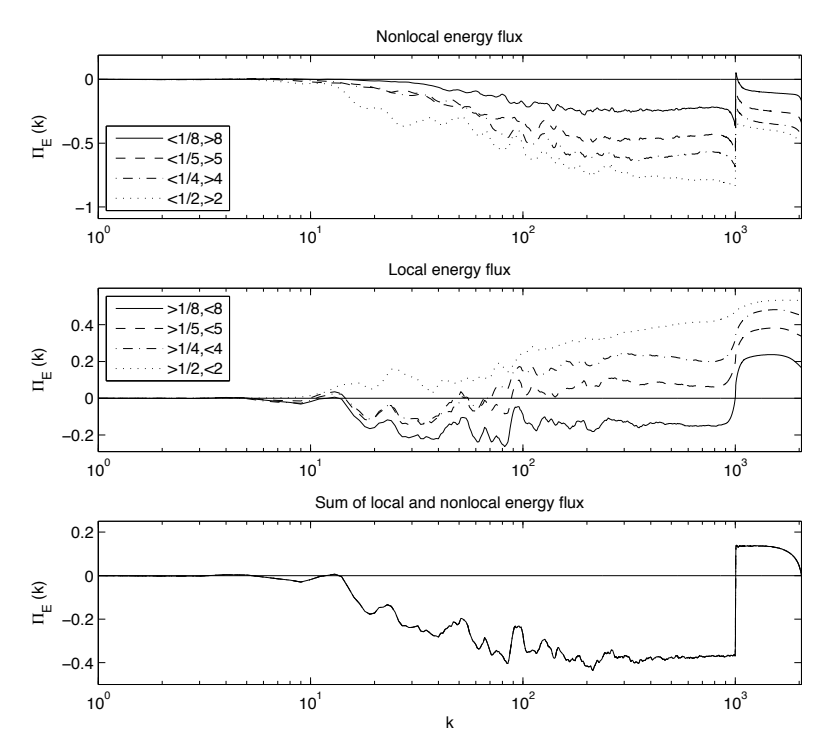


FIGURE 2.10. Energy flux decomposed into nonlocal (top), local (middle) and total (bottom) part for a set of locality thresholds as defined in the text.

nonlocal transfer becomes increasingly important as $Re \to \infty$. Our results may thus be interpreted as a stronger version of Kraichnan's prediction regarding the importance of nonlocal interactions. Already in 1971, Kraichnan found that approximately 60% of the energy transfer comes from wave number triads where the smallest wave number is one fifth of the middle wave number. It can also be noted that a weak coupling between the enstrophy inertial range and the energy-containing scales has been found, giving some support for the observation by Scott (2007). The question regarding the physical mechanisms behind these highly nonlinear interactions in Fourier space is even less settled than the overall mechanisms behind the inverse energy cascade as such.

CHAPTER 3

Quasi-geostrophic turbulence

So far, we have considered two-dimensional turbulence. In many natural systems, such as the atmosphere, there is vertical stratification. Horizontal variations of the density introduces potential energy into the system, which can be released into kinetic energy by the excitation of baroclinic motions. These motions are manifested in the atmosphere by the development of cyclones and anticyclones in the midlatitudes, largely responsible for the day-to-day weather we experience. These systems are generally fully developed at scales $\sim 1000~\rm km$ and can in part be studied within the framework of QG turbulence. This turbulent regime was theoretized by Charney (1971). The dynamics is described by the QG potential vorticity equation, which is given by

$$\frac{\partial q}{\partial t} + (\mathbf{u_h} \cdot \nabla_h) q + \beta v = (-1)^{n+1} \nu_q \nabla^{2n} q + f + (-1)^{p+1} \nu_u \nabla^{-2p} q, \qquad (3.1)$$

where

$$q = \nabla^2 \psi \tag{3.2}$$

is the QG potential vorticity, Δ is the three-dimensional Laplace operator in scaled coordinates, ψ is the stream function, $\mathbf{u_h} = u\mathbf{e_x} + v\mathbf{e_y} = -\partial_y\psi\mathbf{e_x} + \partial_x\psi\mathbf{e_y}$ is the horizontal velocity and ∇_h is the horizontal gradient operator, ν_q is the kinematic viscosity coefficient and ν_u is an optional hypofriction (p>0) or linear drag (p=0) coefficient. For a complete derivation of this equation, see appendix A. The most important property of this equation is the inviscid conservation of potential vorticity. Note also that the quasi-geostrophic motions are in the horizontal plane but that these motions generally vary in the vertical. In the absence of large-scale friction, total energy is also conserved. Thus, there is a very strong link to two-dimensional turbulent characteristics, particularly concerning the directions of the energy and potential enstrophy cascades. The total energy can be divided into kinetic (KE) and potential (PE) energy, which are defined as

$$KE = \frac{1}{2} \int_{V} \left[\left(\frac{\partial \psi}{\partial x} \right)^{2} + \left(\frac{\partial \psi}{\partial y} \right)^{2} \right] dV, \tag{3.3}$$

$$PE = \frac{1}{2} \int_{V} \left[\left(\frac{\partial \psi}{\partial z} \right)^{2} \right] dV, \tag{3.4}$$

respectively, where z denotes the vertical coordinate subject to Charney scaling, i.e, z = N/f Z, where Z is the ordinary Cartesian vertical coordinate.

Following this scaling, Charney argued that the flow field should obey a special type of isotropy, which has been given the name *Charney isotropy*, after Charney (1971). Charney isotropy means that the energy spectrum, in the scaled variables, is invariant in the different directions (i.e., horizontal and vertical). Thus, we can define a Charney isotropy estimate R(k) as

$$R(k) = \frac{E_z(k)}{E_h(k)},\tag{3.5}$$

which should be close to unity, and where $E_z(k)$ and $E_h(k)$ denote the vertical and horizontal energy spectrum, respectively. In analogy with two-dimensional turbulence characteristics, we expect the energy spectrum to scale as k^{-3} in the potential enstrophy inertial range and as $k^{-5/3}$ in the inverse energy cascade range. Charney also predicted approximate equipartition between kinetic and potential energy in the three-dimensional energy spectra. Hence, if we let

$$\phi(k) = \frac{E_k(k)}{E_p(k)} \tag{3.6}$$

denote the degree of equipartition between the three-dimensional kinetic, $E_k(k)$, and potential, $E_p(k)$, energy spectrum, $\phi(k)$ should be close to two, since we have two horizontal velocity components. The prediction of Charney isotropy has been supported by numerical experiments such as Hua & Haidvogel (1986) and McWilliams (1989).

Just as in two-dimensional turbulence, there is rich dynamics in the flow (see figure 3.1), with the development of coherent structures under favourable conditions. The presence of a vertical dimension introduces new features of these vortices, which can be barotropic or baroclinic to various degrees. For a thorough review of their statistical properties, it is recommended to consult, e.g., McWilliams (1990), McWilliams et al. (1999), von Hardenberg et al. (2000) and Reinaud et al. (2003). In paper 4, we present results on a series of high resolution simulations that essentially confirm Charney's predictions under a wide range of conditions and the similarities with 2D turbulence. Furthermore, it is shown that the prediction might even be stronger than Charney anticipated, since the general picture holds qualitatively also in the presence of a planetary vorticity gradient.

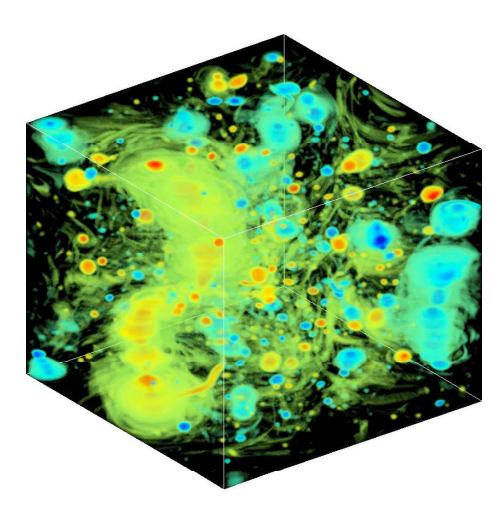


FIGURE 3.1. Potential vorticity snapshot from a freely decaying quasi-geostrophic simulation. Red (blue) colour corresponds to positive (negative) potential vorticity.

CHAPTER 4

Numerical method and the codes

Two pseudospectral codes, PNSE2D and QGE3D, have been developed to solve the two-dimensional Navier-Stokes and the Charney QG potential vorticity equation, respectively. The codes have been written in Fortran 90. Pseudospectral means that the time-stepping is performed in spectral space whereas the nonlinear products are calculated in real space. Fourier transforms are calculated with the aid of an efficient FFT-package called FFTW. Time-stepping is performed with a Runge-Kutta fourth order scheme and the time step is determined using a CFL-condition. Viscosity, being it small scale Navier-Stokes viscosity, hyperviscosity or large scale hypodiffusion or linear friction, is calculated with the use of an integrating factor technique. The codes are essentially free from aliasing errors by the use of an 8/9-dealiasing technique, which allows for a wider range of Fourier modes to be captured compared to the traditional 2/3-dealiasing. For a more thourough review of the details of the codes, see paper 5, which also discusses some statistical measures and parallelisation approaches as well as code performance. It should be noted that the codes have been customized to run on massively parallel super computers, to allow for very high resolution simulations. Figure 4.1 indicates the performance on the Ekman super computer on up to 4096 cpu cores.

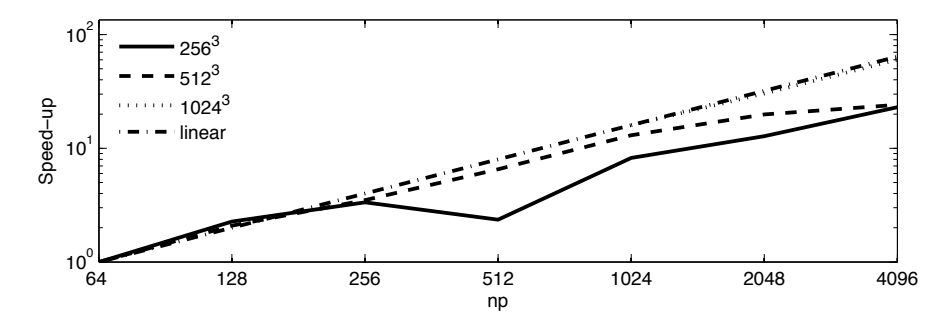


FIGURE 4.1. Speed-up as a function of number of processes (np) for a set of problem sizes on Ekman.

CHAPTER 5

Summary of the papers

Paper 1

The enstrophy cascade in forced two-dimensional turbulence. This paper investigates the enstrophy cascade in forced two-dimensional turbulence through a set of high resolution simulations with different forcing wave numbers. One of the simulations is among the largest simulations presented in the literature so far. In the absence of a large-scale drag, we obtain Kraichnan's original prediction (1967) of a clean k^{-3} energy spectrum in the enstrophy inertial range. However, it is found that the Kraichnan constant varies slightly between the simulations as a consequence of large scale dissipation intermittency. When forcing is applied at relatively large wave number, we obtain coherent vortices at scales larger than the forcing scale, and intermittency measures become very large at all scales. However, when forcing is applied at small wave number, intermittency statistics are close to Gaussian. The main conclusion is that the enstrophy cascade is a robust feature of two-dimensional turbulence but that higher order statistics of vorticity increments lack universality.

Paper 2

Testing Batchelor's similarity hypothesis for decaying two-dimensional turbulence. This paper studies the enstrophy cascade in decaying two-dimensional turbulence to test Batchelor's hypotheses of an equilibrium range and an inertial subrange. Batchelor's hypotheses are corroborated by a set of three simulations with very different initial conditions. As in paper 1, it is found that the Batchelor-Kraichnan constant varies slightly. It is ~ 1.4 in two of the simulations and ~ 1.1 in the other. It is hypothesized that a higher degree of intermittency of dissipation causes the constant to be lower in one of the simulations.

Paper 3

Infrared Reynold's number dependency of the two-dimensional inverse energy cascade. In this paper, the inverse energy cascade is subject to high resolution numerical experiments. A surprising result is obtained, namely that the $k^{-5/3}$ -scaling in the inertial energy range is likely to be a low frictional Reynolds number effect. When the inertial energy range is wide enough, the linear friction is too weak to prevent the formation of coherent vortices. These act to steepen

the energy spectrum from $k^{-5/3}$ to k^{-2} or steeper. The result is strengthened by the somewhat surprising finding that the inverse energy cascade range is maintained by nonlocal triad interactions.

Paper 4

Charney isotropy and equipartition in quasi-geostrophic turbulence. This paper is devoted to studies of quasi-geostrophic turbulence, as theoretized by Charney (1971). We verify Charney's predictions of isotropy and equipartition by performing high resolution three-dimensional simulations. It is demonstrated that Charney's predictions also holds in the presence of a β -effect and in freely decaying quasi-geostrophic turbulence. The analogy with two-dimensional turbulence is investigated and confirmed.

Paper 5

Simulations of two-dimensional and quasi-geostrophic turbulence: Internal Report. This paper is an internal report that describes the two codes in greater detail. The code structures are explored and underlying assumptions, statistical measures and code performance are presented for each code, respectively. The codes are found to scale well in massively parallel systems and they allow for cutting edge numerical experiments.

CHAPTER 6

Outlook

It has become clear that Kraichnan's and Batchelor's predictions on the form of the energy spectrum in the enstrophy inertial range are robust at high Reynolds number. Earlier investigations found a steeper energy spectrum and it was believed to be an effect of intermittency. Our results suggest that intermittency corrections only apply to the Batchelor-Kraichnan constant and not to the k^{-3} -scaling. We now believe we are in a position to interpret this fact as a consequence of the spatial variance of the enstrophy dissipation, as originally addressed by Landau (Landau & Lifshitz 1987). Perhaps of more profound importance is the new evidence of the nonlocality of the inverse energy cascade, which violates the basic assumption of spectral locality of the energy inertial range. It is intriguing to speculate about the consequences of this. Given the two-dimensional nature of quasi-geostrophic turbulence, and the nonlocality of the two-dimensional inverse energy cascade, we may have some disturbing news for the predictability of quasi-geostrophic flows. If the small scales are able to directly communicate with the large scales, by whatever mechanism, we can conjecture that a dynamical analogue to Lorenz butterfly effect is at work in the atmosphere. However, we need to confirm such a conjecture by a careful analysis of the triad interactions in QG flows, which is somewhat more intricate as we also have an interplay between kinetic and potential energy. In addition, the ageostrophic contribution to the potential and kinetic energy spectra along with fluxes of energy and potential enstrophy will be further investigated. Of physical interest, is also to extend the quasi-geostrophic framework to the primitive equations, which are a set of nonlinear equations used in atmospheric and oceanic modeling (Vallis 2006). The set of equations contains the momentum equations in the horizontal, the hydrostatic approximation in the vertical and is completed by the thermodynamic and continuity equations. The use of the primitive equations allows for variations of the Rossby number and deformation radius by varying the stratification, which is fixed in the framework of Charney quasigeostropy. By performing simulations of the primitive equations, we aim to explore the dynamic origins of the atmospheric energy spectrum and, perhaps most importantly, determine the origin of the high wave number $k^{-5/3}$ range in the atmospheric energy spectrum.

Acknowledgements

First of all, I would like to thank my supervisor Dr Erik Lindborg for his guidance, support and openness through the course of my PhD studies 2007-2010. It has been an enjoyable journey, with many good laughs but also a scientific adventure. A true research experience, where nothing has ever been taken for granted, which has lead to many unexpected discoveries. I would also like to thank my co-advisor Geert Brethouwer for his help with getting me started in the implementation of the codes. A great thank you also to Philipp Schlatter, who has given me plenty of good advice in order to increase the performance of the codes, and for carefully reading my code report along with valuable comments. The working environment has been very pleasant thanks to both a good atmosphere in general, and particularly thanks to my PhD student colleagues in the department. A special thank you to my office colleagues Enrico Deusebio and Amin Rasam for sharing thoughts, jokes and the most efficiently used coffee brewer ever, to the best of the author's knowledge. The list would not be complete without a thank you to my colleagues at the Swedish Television, in particular Pär Holmgren and Helen Johansson, who have enabled me to stay in touch with the applied world of meteorology and climate. Something which also Jenny Brandefelt has made possible. Thanks also to Johan Liakka at Stockholm University, whom I have shared thoughts and ideas with every now and then. I would also like to gratefully acknowledge the Linné FLOW centre, financed by the Swedish Research Council (Vetenskapsrådet), for funding of the project. SNIC (Swedish National Infrastructure for Computing) is acknowledged for computer time at the Centre for Parallel Computers (PDC) at the Royal Institute of Technology in Stockholm and the National Supercomputer Centre (NSC) in Linköping, with a generous grant by the Knut and Alice Wallenberg (KAW) foundation. Both computer centres are acknowledged for excellent support. Last, but not the least, I would like to thank all my friends outside of the department, my parents and grandparents, who have always supported me in whatever I have decided to do. At the very last, thank you my dear Liisa for your love, patience and encouragement. It's time for Africa.

APPENDIX A

Derivation of the QG potential vorticity equation

A.1. Introduction

This appendix gives an introduction to the dynamics of the midlatitude troposphere and more specifically to the quasi-geostrophic potential vorticity equation. This is an equation that describes the synoptic scale motions in a bounded domain on a rotating sphere such as the Earth. The aim is to derive a relevant formulation of this equation. The starting point will be the 3D Navier-Stokes equation on a rotating sphere, from which we will systematically exploit the involved terms on our way to quasigeostrophy following Pedlosky (1987).

A.2. Scaling the 3D Navier-Stokes equation

We consider motions on a rotating sphere of radius r_0 , ignoring the slight departure from sphericity of the Earth. We assume that the vertical scale of motion is small enough so that the gravitational acceleration can be considered constant through the depth of the fluid. In addition, we assume that the scales are large enough so that kinematic viscosity can be ignored. Since we can anticipate that the geostrophic approximation must fail near the equator, the theory must apply to a spatial extent that is less than global. Hence, the restriction is that $O\left(\frac{L}{r_0}\right) < 1$. The spherical coordinate system is defined in such a way that the radius \mathbf{r} defines the surface-normal direction, whereas θ is the latitude and ϕ is the longitude. Neglecting viscous effects, friction and forcing, the momentum and mass continuity equations are given by

$$\frac{D\boldsymbol{u}}{Dt} + 2\boldsymbol{\Omega} \times \boldsymbol{u} = -\frac{1}{\rho} \nabla p + \boldsymbol{g}, \tag{A.1}$$

$$\frac{D\rho}{Dt} + \rho \nabla \cdot \boldsymbol{u} = 0, \tag{A.2}$$

$$\frac{D}{Dt} \equiv \frac{\partial}{\partial t} + \boldsymbol{u} \cdot \nabla. \tag{A.3}$$

In spherical coordinates, the mass continuity equation can be expressed as

$$\frac{D\rho}{Dt} + \rho \left[\frac{1}{r^2} \frac{\partial (r^2 w)}{\partial r} + \frac{1}{r \cos \theta} \frac{\partial (v \cos \theta)}{\partial \theta} + \frac{1}{r \cos \theta} \frac{\partial u}{\partial \phi} \right] = 0, \tag{A.4}$$

$$\frac{D}{Dt} = \frac{\partial}{\partial t} + \frac{u}{r\cos\theta} \frac{\partial}{\partial \phi} + \frac{v}{r} \frac{\partial}{\partial \theta} + w \frac{\partial}{\partial r}.$$
 (A.5)

Now let

 $\boldsymbol{u} = u\hat{\boldsymbol{\phi}} + v\hat{\boldsymbol{\theta}} + w\hat{\boldsymbol{r}}.$ (A.6)

$$u \equiv r \cos \theta \frac{D\phi}{Dt},\tag{A.7}$$

$$v \equiv r \frac{D\theta}{Dt},\tag{A.8}$$

$$w \equiv \frac{Dr}{Dt}.\tag{A.9}$$

Hence,

$$\frac{D\boldsymbol{u}}{Dt} = \hat{\boldsymbol{\phi}} \frac{D\boldsymbol{u}}{Dt} + \hat{\boldsymbol{\theta}} \frac{D\boldsymbol{v}}{Dt} + \hat{\boldsymbol{r}} \frac{D\boldsymbol{w}}{Dt} + u \frac{D\hat{\boldsymbol{\phi}}}{Dt} + v \frac{D\hat{\boldsymbol{\theta}}}{Dt} + w \frac{D\hat{\boldsymbol{r}}}{Dt}. \tag{A.10}$$

Similarity consideration shows that

$$\lim_{\delta x \to 0} \frac{|\delta \hat{\phi}|}{\delta x} = \frac{1}{r \cos \theta},\tag{A.11}$$

$$\frac{\delta \hat{\boldsymbol{\phi}}}{\delta x} = \frac{1}{r \cos \theta} \left(\hat{\boldsymbol{\theta}} \sin \theta - \hat{\boldsymbol{r}} \cos \theta \right), \tag{A.12}$$

$$\frac{D\hat{\phi}}{Dt} = \frac{u}{r\cos\theta} \left(\hat{\boldsymbol{\theta}}\sin\theta - \hat{\boldsymbol{r}}\cos\theta \right), \tag{A.13}$$

and equivalently for the $\hat{\theta}$ and \hat{r} unit vectors it can be shown that

$$\frac{D\hat{\boldsymbol{\theta}}}{Dt} = -\frac{u\tan\theta}{r}\hat{\boldsymbol{\phi}} - \frac{v}{r}\hat{\boldsymbol{r}},\tag{A.14}$$

$$\frac{D\hat{r}}{Dt} = \frac{u}{r}\hat{\phi} + \frac{v}{r}\hat{\theta}.$$
 (A.15)

Thus, the acceleration following the relative motion in spherical coordinates is given by

$$\frac{D\boldsymbol{u}}{Dt} = \hat{\boldsymbol{\phi}} \left(\frac{D\boldsymbol{u}}{Dt} - \frac{\boldsymbol{u}\boldsymbol{v}\tan\theta}{r} + \frac{\boldsymbol{u}\boldsymbol{w}}{r} \right) + \hat{\boldsymbol{\theta}} \left(\frac{D\boldsymbol{v}}{Dt} + \frac{\boldsymbol{u}^2\tan\theta}{r} + \frac{\boldsymbol{v}\boldsymbol{w}}{r} \right) + \hat{\boldsymbol{r}} \left(\frac{D\boldsymbol{w}}{Dt} - \frac{\boldsymbol{u}^2 + \boldsymbol{v}^2}{r} \right). \tag{A.16}$$

Expansion of the Coriolis term in spherical coordinates is given below;

$$2\mathbf{\Omega} \times \mathbf{u} = 2\Omega \begin{vmatrix} \hat{\boldsymbol{\phi}} & \hat{\boldsymbol{\theta}} & \hat{\boldsymbol{r}} \\ 0 & \cos \theta & \sin \theta \\ u & v & w \end{vmatrix} = 2\Omega \left[(w\cos \theta - v\sin \theta) \,\hat{\boldsymbol{\phi}} + u\sin \theta \,\hat{\boldsymbol{\theta}} - u\cos \theta \,\hat{\boldsymbol{r}} \right].$$
(A.17)

The pressure gradient and gravity are trivially expressed and can easily be identified in the component form of (A.1), as shown below:

$$\frac{Du}{Dt} + \frac{uw}{r} - \frac{uv}{r}\tan\theta + 2\Omega w\cos\theta - 2\Omega v\sin\theta = -\frac{1}{\rho r\cos\theta}\frac{\partial p}{\partial \phi}, \quad (A.18)$$

$$\frac{Dv}{Dt} + \frac{vw}{r} + \frac{u^2}{r}\tan\theta + 2\Omega u\sin\theta = -\frac{1}{\rho r}\frac{\partial p}{\partial \theta},$$
 (A.19)

$$\frac{Dw}{Dt} - \frac{u^2 + v^2}{r} - 2\Omega u \cos \theta = -\frac{1}{\rho} \frac{\partial p}{\partial r} - g.$$
 (A.20)

The momentum and mass continuity equation need to be complemented by the thermodynamic equation;

$$\frac{D\theta}{Dt} = \frac{\theta}{c_p T} \left(\frac{k}{\rho} \nabla^2 T + Q \right), \tag{A.21}$$

where k is the thermal conductivity, T the temperature, Q the rate of heat addition per unit mass by internal heat sources and θ is the potential temperature, defined as

$$\theta = T \left(\frac{p_0}{p}\right)^{\frac{R}{c_p}}. (A.22)$$

Note that p, ρ and T are related by the ideal gas law;

$$p = \rho RT. \tag{A.23}$$

Now, we consider motions, whose horizontal spatial scale of variation is given by the length scale L and velocity scale U. Furthermore, we restrict ourselves to the mid-latitude region centred at around some latitude θ_0 . In addition, we switch to Cartesian coordinates by replacing the spherical coordinates as follows

$$\begin{cases} x = \phi r_0 \cos \theta_0, \\ y = r_0(\theta - \theta_0), \end{cases}$$
 (A.24)

and hence

$$\begin{cases} \frac{\partial}{\partial \phi} = r_0 \cos \theta_0 \frac{\partial}{\partial x}, \\ \frac{\partial}{\partial \theta} = r_0 \frac{\partial}{\partial y}. \end{cases}$$
 (A.25)

In addition, the following substitutions are introduced

$$\begin{cases}
z = r - r_0 = Dz', \\
x = Lx', \\
y = Ly', \\
t = \frac{L}{U}t', \\
u = Uu', \\
v = Uv', \\
w = \frac{D}{L}Uw'.
\end{cases}$$
(A.26)

Note that the time scales advectively. We now turn to the hydrostatic approximation;

$$\frac{\partial p_s}{\partial z} = -\rho_s(z)g,\tag{A.27}$$

where the subscript s denotes a standard basic state upon which perturbations occur such that

$$\begin{cases}
p = p_s(z) + \tilde{p}(x, y, z, t), \\
\rho = \rho_s(z) + \tilde{\rho}(x, y, z, t).
\end{cases}$$
(A.28)

We need to scale the pressure and density pertubations in some sense. It can be conjectured that for the motions of interest, the horizontal pressure gradient will be of the same order of magnitude as the Coriolis acceleration, i.e., $\mathcal{O}(\rho_s 2\Omega u \sin \theta_0) \sim \mathcal{O}\left(\frac{\tilde{p}}{L}\right) \rightarrow \tilde{p} \sim \mathcal{O}(\rho_s U f_0 L)$, where

$$f_0 = 2\Omega \sin \theta_0, \tag{A.29}$$

is the Coriolis parameter at θ_0 . Hence,

$$p = p_s(z) + \rho_s(z)Uf_0Lp'. \tag{A.30}$$

In a similar manner, we may anticipate that the buoyancy force due to $\tilde{\rho}$ will be of the same order of magnitude as the vertical pressure gradient by recalling the hydrostatic approximation, upon which $\frac{\partial \tilde{p}}{\partial z} = \mathcal{O}\left(\frac{\tilde{p}}{D}\right) = \mathcal{O}\left(\frac{\rho_s U f_0 L}{D}\right) \sim$

$$\mathcal{O}(\tilde{\rho}g) \to \mathcal{O}(\tilde{\rho}) = \mathcal{O}\left(\rho_s U \frac{f_0 L}{gD}\right)$$
. Hence, we may write

$$\rho = \rho_s(z) \left[1 + Ro \ F \rho' \right], \tag{A.31}$$

where

$$\begin{cases}
Ro \equiv \frac{U}{f_0 L} \equiv \epsilon, \\
F = \frac{f_0^2 L^2}{gD}.
\end{cases}$$
(A.32)

Here, $Ro = \epsilon$ is the Rossby number. We are now at the point where the momentum equation components can be non-dimensionalized following the substitutions addressed so far. Thus, applying (A.26), (A.27), (A.30) and (A.31) to the component momentum equations and dividing through by Uf_0 , we obtain

$$\epsilon \left[\frac{Du'}{Dt'} + \frac{L}{r_*} \left(\delta u' w' - u' v' \tan \theta \right) \right] - v' \frac{\sin \theta}{\sin \theta_0} + \delta w' \frac{\cos \theta}{\sin \theta_0} =$$

$$= -\frac{r_0}{r_*} \frac{\cos \theta_0}{\cos \theta} \frac{1}{1 + \epsilon F \rho'} \frac{\partial p'}{\partial x'}, \quad (A.33)$$

$$\epsilon \left[\frac{Dv'}{Dt'} + \frac{L}{r_*} \left(\delta v'w' + u'^2 \tan \theta \right) \right] + u' \frac{\sin \theta}{\sin \theta_0} = -\frac{r_0}{r_*} \frac{1}{1 + \epsilon F \rho'} \frac{\partial p'}{\partial y'}, \quad (A.34)$$

$$D(1 + \epsilon F \rho') \left[U^2 \left(\frac{D}{L^2} \frac{Dw'}{Dt'} - \frac{u'^2 + v'^2}{r_*} \right) - 2\Omega U u' \cos \theta \right] =$$

$$= -\frac{1}{\rho_s} \frac{\partial}{\partial z'} \left[p_s + U f_0 L \rho_s p' \right] - D(1 + \epsilon F \rho') g_*, \quad (A.35)$$

where the subscript * denotes dimensional quantities and

$$\delta \equiv \frac{D}{L}.\tag{A.36}$$

The vertical component (A.35) can be further simplified by expansion of the right hand side, to yield, after division by Uf_0L ;

$$(1 + \epsilon F \rho') \left[\epsilon \delta^2 \frac{Dw'}{Dt'} - \frac{\epsilon \delta L}{r_*} (u'^2 + v'^2) - \delta u' \frac{\cos \theta}{\sin \theta_0} \right] = -\frac{1}{\rho_s} \frac{\partial}{\partial z'} (\rho_s p') - \rho'.$$
(A.37)

The nondimenzionalized total derivative takes the following form

$$\frac{D}{Dt'} = \frac{\partial}{\partial t'} + u' \frac{r_0}{r_*} \frac{\cos \theta_0}{\cos \theta} \frac{\partial}{\partial x'} + v' \frac{r_0}{r_*} \frac{\partial}{\partial y'} + w' \frac{\partial}{\partial z'}.$$
 (A.38)

Note that

$$\frac{r_*}{r_0} = 1 + \delta\left(\frac{L}{r_0}\right)z'. \tag{A.39}$$

Expanding the mass continuity equation (A.4) and applying the substitutions result in the nondimensional version

$$\epsilon F \frac{D\rho'}{Dt'} + (1 + \epsilon F \rho') \left[\frac{w'}{\rho_s} \frac{\partial \rho_s}{\partial z'} + \frac{\partial w'}{\partial z'} + 2 \frac{D}{r_*} w' + \frac{r_0}{r_*} \frac{\partial v'}{\partial y'} + \frac{L}{r_*} \frac{v' \tan \theta}{\cos \theta} \frac{\partial u'}{\partial x'} \right] = 0. \quad (A.40)$$

In the following, the superscripts' denoting the nondimensional variables will be dropped and the subscript * will denote dimensional remnants in the equations. It is important to note that no restrictive approximations have been applied so far. The equations have just been scaled so that their relative magnitude can be estimated by the nondimensional parameters multiplying the individual terms. Before investigating any specific parameter settings, we expand the trigonometric terms around the θ_0 -latitude in Taylor expansions, i.e.,

$$\sin \theta = \sin \theta_0 + \frac{d(\sin \theta)}{d\theta}|_{\theta = \theta_0} (\theta - \theta_0) + \frac{d^2(\sin \theta)}{d\theta^2}|_{\theta = \theta_0} \frac{(\theta - \theta_0)^2}{2!} + \dots \quad (A.41)$$

With the use of (A.24) and (A.26) we thus obtain

$$\begin{cases} \sin \theta = \sin \theta_0 + \frac{L}{r_0} y \cos \theta_0 - \frac{1}{2} \left(\frac{L}{r_0}\right)^2 y^2 \sin \theta_0 + \dots, \\ \cos \theta = \cos \theta_0 - \frac{L}{r_0} y \sin \theta_0 - \frac{1}{2} \left(\frac{L}{r_0}\right)^2 y^2 \cos \theta_0 + \dots, \\ \tan \theta = \tan \theta_0 + \frac{L}{r_0} y \frac{1}{\cos^2 \theta_0} + \left(\frac{L}{r_0}\right)^2 y^2 \frac{\tan \theta_0}{\cos^2 \theta_0} + \dots, \end{cases}$$
(A.42)

Last, but not the least, we now define the β -parameter as

$$\beta_0 = \frac{d}{dy} \left(2\Omega \sin \theta \right) |_{\theta = \theta_0} = \frac{1}{r_0} \frac{d}{d\theta} \left(2\Omega \sin \theta \right) |_{\theta = \theta_0} = \frac{2\Omega}{r_0} \cos \theta_0 \tag{A.43}$$

It can be noted here that $\frac{\beta_0 L}{f_0} = \dots = \frac{L}{r_0} \cot \theta_0 \sim \mathcal{O}\left(\frac{L}{r_0}\right)$ and hence $\frac{\beta_0 L}{f_0} = \frac{\beta_0 L^2}{U} \sim \mathcal{O}\left(\frac{L}{\epsilon r_0}\right)$ so that the magnitude of the relative vorticity- to the planetary

vorticity gradient is measured by

$$\frac{1}{\beta} = \frac{U}{\beta_0 L^2} \sim \mathcal{O}\left(\epsilon \frac{r_0}{L}\right),\tag{A.44}$$

which is evidentally determined by the relative size of the Rossby number and the inverse ratio between the horizontal length scale and approximately the Earth's radius for tropospheric considerations.

A.3. The geostrophic approximation

So far, no specific scale of motion has been chosen. By noting that in the midlatitude atmosphere,

$$\begin{cases}
U \sim \mathcal{O}(10 \ ms^{-1}), \\
L \sim \mathcal{O}(1000 \ km), \\
D \sim \mathcal{O}(10 \ km), \\
f_0 \sim \mathcal{O}(10^{-4} \ s^{-1}),
\end{cases}$$
(A.45)

we first choose to study the case $\epsilon \sim \mathcal{O}\left(\frac{L}{r_0} << 1\right)$, i.e., motions that are less than global. Under these circumstances, $\frac{U}{\beta_0 L^2} \sim \mathcal{O}\left(\frac{10}{10^{-11}(10^6)^2}\right) \sim \mathcal{O}(1)$. Thus, the planetary vorticity gradient is expected to play an active role in the atmospheric dynamics at this horizontal length scale. Making use of (A.45), we can summarize the key parameters as

$$\begin{cases} \epsilon \sim \mathcal{O}(10^{-1}), \\ \beta \sim \mathcal{O}(1), \\ F = \frac{f_0^2 L^2}{gD} \sim \mathcal{O}(10^{-1}) \sim O(\epsilon), \\ \frac{L}{r_0} \sim \mathcal{O}(\epsilon), \\ \delta = \frac{D}{L} \sim \mathcal{O}(10^{-2}) \sim \mathcal{O}(\epsilon^2), \\ \frac{r_*}{r_0} - 1 \sim \mathcal{O}\left(\delta \frac{L}{r_0}\right) \sim \mathcal{O}(\epsilon^3), \end{cases}$$
(A.46)

The limit $\epsilon \to 0$, $\frac{\epsilon r_0}{L} \sim \mathcal{O}(1)$, is a special case that examines geostrophic dynamics when the planetary vorticity gradient contributes equally to the relative vorticity gradient. We now express all the dynamic variables, i.e., u, v, w, p, ρ , in series of the key parameter ϵ such that

$$u(x, y, z, t) = u_0(x, y, z, t) + \epsilon u_1(x, y, z, t) + \epsilon^2 u_2(x, y, z, t) + \dots etc. \quad (A.47)$$

Applying (A.42), (A.46) and the first two terms of (A.47) for the dynamic variables to (A.33), (A.34) and (A.37), we obtain

$$\epsilon \left[\frac{D(u_0 + \epsilon u_1)}{Dt} + \frac{L}{r_*} \left(\epsilon^2 (u_0 + \epsilon u_1)(w_0 + \epsilon w_1) + \frac{L}{r_0} \cos^{-2} \theta_0 \right) \right] + \\
- (u_0 + \epsilon u_1)(v_0 + \epsilon v_1) \left(\tan \theta_0 + \frac{Ly}{r_0} \cos^{-2} \theta_0 \right) \right] + \\
- (v_0 + \epsilon v_1) \frac{\left(\sin \theta_0 + \frac{Ly}{r_0} \cos \theta_0 \right)}{\sin \theta_0} + \epsilon (w_0 + \epsilon w_1) \frac{\left(\cos \theta_0 - \frac{Ly}{r_0} \sin \theta_0 \right)}{\sin \theta_0} = \\
= -\frac{r_0}{r_*} \frac{\cos \theta_0}{\left(\cos \theta_0 - \frac{Ly}{r_0} \sin \theta_0 \right)} \frac{1}{1 + \epsilon^2 (\rho_0 + \epsilon \rho_1)} \frac{\partial (p_0 + \epsilon p_1)}{\partial x}, \quad (A.48)$$

$$\epsilon \left[\frac{D(v_0 + \epsilon v_1)}{Dt} + \frac{L}{r_*} \left(\epsilon^2 (v_0 + \epsilon v_1)(w_0 + \epsilon w_1) + \left(u_0 + \epsilon u_1 \right)^2 \left(\tan \theta_0 + \frac{Ly}{r_0} \cos^{-2} \theta_0 \right) \right) \right] + (u_0 + \epsilon u_1) \frac{\left(\sin \theta_0 + \frac{Ly}{r_0} \cos \theta_0 \right)}{\sin \theta_0} = \\
= -\frac{r_0}{r_*} \frac{1}{1 + \epsilon^2 (\rho_0 + \epsilon \rho_1)} \frac{\partial (p_0 + \epsilon p_1)}{\partial y}, \quad (A.49)$$

$$\left(1 + \epsilon^2(\rho_0 + \epsilon \rho_1)\right) \left[\epsilon^5 \frac{D(w_0 + \epsilon w_1)}{Dt} - \frac{\epsilon^3 L}{r_*} \left((u_0 + \epsilon u_1)^2 + (v_0 + \epsilon v_1)^2 \right) + \right. \\
\left. - \epsilon^2 (u_0 + \epsilon u_1) \frac{\left(\cos \theta_0 - \frac{Ly}{r_0} \sin \theta_0\right)}{\sin \theta_0} \right] = \\
= -\frac{1}{\rho_s} \frac{\partial}{\partial z} \left(\rho_s(p_0 + \epsilon p_1) \right) - (\rho_0 + \epsilon \rho_1), \quad (A.50)$$

The mass continuity equation (A.40) takes the form

$$\epsilon^{2} \frac{D(\rho_{0} + \epsilon \rho_{1})}{Dt} + \left(1 + \epsilon^{2} (\rho_{0} + \epsilon \rho_{1})\right) \left[\frac{w_{0} + \epsilon w_{1}}{\rho_{s}} \frac{\partial \rho_{s}}{\partial z} + \frac{\partial (w_{0} + \epsilon w_{1})}{\partial z} + \frac{D}{2} (w_{0} + \epsilon w_{1}) + \frac{r_{0}}{r_{*}} \frac{\partial (v_{0} + \epsilon v_{1})}{\partial y} - \frac{L}{r_{*}} (v_{0} + \epsilon v_{1}) \left(\tan \theta_{0} + \frac{Ly}{r_{0}} \cos^{-2} \theta_{0}\right) + \frac{r_{0}}{r_{*}} \frac{\cos \theta_{0}}{\cos \theta_{0} - \frac{Ly}{r_{0}} \sin \theta_{0}} \frac{\partial (u_{0} + \epsilon u_{1})}{\partial x}\right] = 0. \quad (A.51)$$

If we note that $\mathcal{O}\left(\frac{D}{r_*}\right) < \mathcal{O}(\epsilon^2)$, and establish that terms of like order in ϵ must balance, we obtain, to first order,

$$\begin{cases} v_0 = \frac{\partial p_0}{\partial x}, \\ u_0 = -\frac{\partial p_0}{\partial y}, \\ \rho_0 = -\frac{1}{\rho_s} \frac{\partial}{\partial z} \left(p_0 \rho_s \right), \\ \frac{1}{\rho_s} \frac{\partial (w_0 \rho_s)}{\partial z} + \frac{\partial u_0}{\partial x} + \frac{\partial v_0}{\partial y} = 0. \end{cases}$$
(A.52)

The equation set (A.52) is the geostrophic approximation. The $\mathcal{O}(1)$ motion is thus determined by the horizontal pressure gradient. Furthermore, it can be established that the $\mathcal{O}(1)$ geostrophic velocities are horizontally nondivergent, since

$$\frac{\partial v_0}{\partial y} + \frac{\partial u_0}{\partial x} = 0, \tag{A.53}$$

which implies that

$$\frac{\partial}{\partial z}(\rho_s w_0) = 0. \tag{A.54}$$

Hence, $\rho_s w_0$ is independent of z and if $w_0 = 0$ for any z, it will be zero $\forall z$, e.g., if the domain is bounded below or above. Thus, the vertical velocity is given by

$$w(x, y, z, t) = \epsilon w_1(x, y, z, t) + \epsilon^2 w_2(x, y, z, t) + \dots$$
 (A.55)

which is a direct consequence of the geostrophic approximation. Therefore, we cannot determine p_0 and hence u_0 and v_0 without considering higher order dynamics. The $\mathcal{O}(\epsilon)$ terms with the use of (A.55) are given below, starting with the zonal component

$$\frac{Du_0}{Dt} - \frac{Ly}{\epsilon r_0} v_0 \cot \theta_0 - v_1 = -\frac{\partial p_1}{\partial x} - \frac{Ly}{\epsilon r_0} \tan \theta_0 \frac{\partial p_0}{\partial x}, \tag{A.56}$$

where the second term on the right hand side was obtained by a little manipulation;

$$-\frac{r_0}{r_*} \frac{\cos \theta_0}{\cos \theta_0 - \frac{Ly}{r_0} \sin \theta_0} \frac{\partial p_0}{\partial x} =$$

$$= -\frac{r_0}{r_*} \frac{\cos \theta_0 \left(\cos \theta_0 + \frac{Ly}{r_0} \sin \theta_0\right)}{\left(\cos \theta_0 - \frac{Ly}{r_0} \sin \theta_0\right) \left(\cos \theta_0 + \frac{Ly}{r_0} \sin \theta_0\right)} \frac{\partial p_0}{\partial x} =$$

$$= -\frac{r_0}{r_*} \frac{\cos^2 \theta_0 + \frac{Ly}{r_0} \cos \theta_0 \sin \theta_0}{\cos^2 \theta_0 - \left(\frac{L}{r_0}\right)^2 y^2 \sin^2 \theta_0} \frac{\partial p_0}{\partial x} \approx \frac{L}{r_*} y \tan \theta_0 \frac{\partial p_0}{\partial x} \quad Q.E.D. \quad (A.57)$$

The meridional $\mathcal{O}(\epsilon)$ component is given by

$$\frac{Dv_0}{Dt} + u_0 \frac{Ly}{\epsilon r_0} \cot \theta_0 + u_1 = -\frac{\partial p_1}{\partial y}.$$
 (A.58)

The total derivative is given by

$$\frac{D}{Dt} = \frac{\partial}{\partial t} + (u_0 + \epsilon u_1) \frac{r_0}{r_*} \frac{\cos \theta_0}{\cos \theta_0 - \frac{Ly}{r_0} \sin \theta_0} \frac{\partial}{\partial x} + (v_0 + \epsilon v_1) \frac{r_0}{r_*} \frac{\partial}{\partial y} + \epsilon w_1 \frac{\partial}{\partial z}, \quad (A.59)$$

so that (A.56) and (A.58) become

$$\begin{cases}
\frac{\partial u_0}{\partial t} + u_0 \frac{\partial u_0}{\partial x} + v_0 \frac{\partial u_0}{\partial y} - v_1 - v_0 \frac{Ly}{\epsilon r_0} \cot \theta_0 = -\frac{\partial p_1}{\partial x} - \frac{Ly}{\epsilon r_0} \tan \theta_0 \frac{\partial p_0}{\partial x}, \\
\frac{\partial v_0}{\partial t} + u_0 \frac{\partial v_0}{\partial x} + v_0 \frac{\partial v_0}{\partial y} + u_1 + u_0 \frac{Ly}{\epsilon r_0} \cot \theta_0 = -\frac{\partial p_1}{\partial y}.
\end{cases}$$
(A.60)

We complete with the mass continuity equation:

$$\frac{1}{\rho_s} \frac{\partial}{\partial z} (\rho_s w_1) + \frac{\partial u_1}{\partial x} + \frac{\partial v_1}{\partial y} - v_0 \frac{L}{\epsilon r_0} \tan \theta_0 + \frac{Ly}{\epsilon r_0} \tan \theta_0 \frac{\partial u_0}{\partial x} = 0.$$
 (A.61)

Pedlosky (1987) discusses the presence of terms that are $\sim \frac{L}{\epsilon r_0}$ in the momentum equation (A.60), and notes that these terms on the left hand side are due to the variation of the Coriolis parameter on a β -plane whereas on the right hand side, these terms reflect the variation of the metric term $\cos \theta$. If $\tan \theta_0$ would be small, this term would be negligible. Then (A.60) would reduce to the $\mathcal{O}(\epsilon)$ momentum equation for a flat Earth with a linearly varying Coriolios parameter in the meridional direction. However, this would push the domain to latitudes near the equator, where the theory fails. Thus, a model of a flat Earth with sphericity accounted for only by a varying f is not valid for the $\mathcal{O}(\epsilon)$ momentum balance. Pedlosky (1987) states however, that the β -plane approximation only requires that the vorticity equation satisfies the β -plane approximation. By taking $-\frac{\partial}{\partial y}$ (A.60 a) $+\frac{\partial}{\partial x}$ (A.60 b), and noting that the relative vorticity is given by

$$\zeta_0 = \frac{\partial v_0}{\partial x} - \frac{\partial u_0}{\partial y},\tag{A.62}$$

we yield after some simplification that

$$\begin{split} \frac{\partial \zeta_0}{\partial t} + u_0 \frac{\partial \zeta_0}{\partial x} + v_0 \frac{\partial \zeta_0}{\partial y} + \left(\frac{\partial u_1}{\partial x} + \frac{\partial v_1}{\partial y} \right) + v_0 \frac{L}{\epsilon r_0} \cot \theta_0 = \\ &= \frac{L}{\epsilon r_0} \tan \theta_0 \frac{\partial p_0}{\partial x} + \frac{Ly}{\epsilon r_0} \tan \theta_0 \frac{\partial^2 p_0}{\partial x \partial y}, \quad (A.63) \end{split}$$

where use have been made of the nondivergence of the $\mathcal{O}(1)$ -momentum. We can simplify this further by taking advantage of the fact that

$$\frac{1}{\beta} = \frac{U}{\beta_0 L^2} = \frac{U}{\frac{f_0}{r_0} L^2 \cot \theta_0} = \left[\frac{L}{r_0} \sim \epsilon\right] = \frac{U}{\epsilon f_0 L \cot \theta_0} = \left[\frac{U}{f_0 L} \sim \epsilon\right] = \frac{1}{\cot \theta_0},\tag{A.64}$$

upon which we obtain

$$\frac{\partial \zeta_0}{\partial t} + u_0 \frac{\partial \zeta_0}{\partial x} + v_0 \frac{\partial \zeta_0}{\partial y} + \beta v_0 = \frac{L}{\epsilon r_0} \left[\tan \theta_0 \frac{\partial p_0}{\partial x} + y \tan \theta_0 \frac{\partial^2 p_0}{\partial x \partial y} \right] - \left(\frac{\partial u_1}{\partial x} + \frac{\partial v_1}{\partial y} \right). \tag{A.65}$$

From the geostrophic approximation (A.52), the mass continuity equation (A.61) can be rewritten as

$$\frac{1}{\rho_s} \frac{\partial(\rho_s w_1)}{\partial z} + \left(\frac{\partial u_1}{\partial x} + \frac{\partial v_1}{\partial y}\right) - \frac{L}{\epsilon r_0} \tan \theta_0 \frac{\partial p_0}{\partial x} - \frac{Ly}{\epsilon r_0} \tan \theta_0 \frac{\partial^2 p_0}{\partial x \partial y} = 0, \quad (A.66)$$

from which we clearly can rewrite (A.65) as

$$\frac{D_0}{Dt} \left[\zeta_0 + \beta y \right] = \frac{1}{\rho_s} \frac{\partial (\rho_s w_1)}{\partial z},\tag{A.67}$$

where

$$\frac{D_0}{Dt} \equiv \frac{\partial}{\partial t} + u_0 \frac{\partial}{\partial x} + v_0 \frac{\partial}{\partial y}.$$
 (A.68)

It is now clear that (A.67) is the vorticity equation for a flat Earth model with a linearly varying Coriolis parameter in the meridional direction. The $\mathcal{O}(1)$ velocity field is determined in terms of p_0 by the $\mathcal{O}(1)$ momentum equation so that

$$\zeta_0 = \frac{\partial^2 p_0}{\partial x^2} + \frac{\partial^2 p_0}{\partial y^2}.$$
 (A.69)

However, we still need to resolve w_1 , which requires the use of the thermodynamic equation.

A.4. Using static stability to resolve the vertical motion

To complete the derivation of the quasi-geostrophic motions we need to to represent ϵw_1 in terms of the $\mathcal{O}(1)$ geostrophic fields. This will be possible by making use of the thermodynamic equation. By considering adiabatic motions, the potential temperature θ (see A.22), is conserved. By making use of the ideal gas law (A.23), θ can be rewritten as

$$\theta = \frac{p}{\rho R} \left(\frac{p_0}{p} \right)^{\frac{R}{c_p}} \Longleftrightarrow \rho = \frac{p}{R\theta} \left(\frac{p_0}{p} \right)^{\frac{R}{c_p}} = \frac{p}{R\theta} \left(\frac{p}{p_0} \right)^{\frac{1}{\gamma}}, \tag{A.70}$$

where

$$\gamma \equiv \frac{c_p}{c_n}.\tag{A.71}$$

If we consider vertical displacement of an air parcel between a lower level z (A) to an upper level z + dz (B), the density of parcel A will have changed by an amount

$$\Delta \rho_A = \frac{1}{\gamma} \frac{p_0}{R\theta} \left(\frac{p}{p_0}\right)^{\frac{1}{\gamma}} \frac{\partial p}{\partial z} \frac{dz}{p}.$$
 (A.72)

Hence, the new density at z + dz is thus

$$\rho_A + \Delta \rho_A = \rho_A(z) + \frac{1}{\gamma} \frac{\rho}{p} \frac{\partial p}{\partial z} dz. \tag{A.73}$$

However, the density of parcel B at z+dz in terms of the undisturbed density A had at z, is given by

$$\rho_B = \rho_A(z) + \frac{\partial \rho}{\partial z} dz. \tag{A.74}$$

The excess density of A at z + dz is

$$(\rho_A + \Delta \rho_A) - \rho_B = \left(\frac{1}{\gamma} \frac{\rho}{p} \frac{\partial p}{\partial z} - \frac{\partial \rho}{\partial z}\right) dz, \tag{A.75}$$

which causes a restoring force

$$\frac{g}{\rho} (\rho_A + \Delta \rho_A - \rho_B) = g \left(\frac{1}{\gamma} \frac{\rho}{p} \frac{\partial p}{\partial z} - \frac{\partial \rho}{\partial z} \right) dz =
= g \left[\frac{1}{\gamma p} \frac{\partial p}{\partial z} - \frac{R\theta}{p_0} \left(\frac{p}{p_0} \right)^{-\frac{1}{\gamma}} \frac{\partial}{\partial z} \left(\frac{p_0}{R\theta} \left(\frac{p}{p_0} \right)^{\frac{1}{\gamma}} \right) \right] dz =
= g \left[\frac{1}{\gamma p} \frac{\partial p}{\partial z} - \frac{R\theta}{p_0} \left(\frac{p}{p_0} \right)^{-\frac{1}{\gamma}} \left(-\frac{1}{\theta^2} \frac{\partial \theta}{\partial z} \left(\frac{p}{p_0} \right)^{\frac{1}{\gamma}} \frac{p_0}{R} + \frac{p_0}{\gamma \theta p R} \left(\frac{p}{p_0} \right)^{\frac{1}{\gamma}} \frac{\partial p}{\partial z} \right) \right] dz =
= g \left(\frac{1}{\theta} \frac{\partial \theta}{\partial z} \right) dz \quad (A.76)$$

Thus, if $\frac{\partial \theta}{\partial z} > 0$, the buoyancy force is restoring and the static state is stable with respect to small adiabatic displacements. The static stability is defined as

$$\sigma = \frac{1}{\theta} \frac{\partial \theta}{\partial z},\tag{A.77}$$

and the fluid parcel oscillation frequency is defined by

$$N \equiv \left(\frac{g}{\theta} \frac{\partial \theta}{\partial z}\right)^{\frac{1}{2}},\tag{A.78}$$

which is commonly referred to as the Brunt-Väisälä frequency. From the definition of θ , it can be found that

$$\frac{1}{\theta} \frac{\partial \theta}{\partial z} = \frac{1}{T} \left[\frac{\partial T}{\partial z} + \frac{g}{c_p} \right],\tag{A.79}$$

if the hydrostatic approximation $\left(\frac{\partial p}{\partial z} = -\rho g\right)$ is used. Hence, if $\frac{\partial T}{\partial z} < 0$, the atmosphere will be statically stable as long as the lapse rate, $-\frac{\partial T}{\partial z} < \frac{g}{c_p}$. Finally we note that for the atmosphere, $N \sim \mathcal{O}(10^{-2}s^{-1})$.

A.5. The quasi-geostrophic potential vorticity equation

Recalling (A.70), we note that (in dimensional form)

$$\ln \rho = \ln \left[\frac{p_0}{R\theta} \left(\frac{p}{p_0} \right)^{\frac{1}{\gamma}} \right] \iff$$

$$\ln \rho = \ln \left(\frac{p_0}{R\theta} \right) + \frac{1}{\gamma} \ln \left(\frac{p}{p_0} \right) \iff$$

$$\ln \rho = \ln p_0 - \ln R - \ln \theta + \frac{1}{\gamma} \ln p - \frac{1}{\gamma} \ln p_0 \iff$$

$$\ln \theta = \frac{1}{\gamma} \ln p - \ln \rho + \left(1 - \frac{1}{\gamma} \right) \ln p_0 - \ln R \iff \left[\gamma = \frac{c_p}{c_v} \; ; \; c_p = c_v + R \right] \iff$$

$$\ln \theta = \frac{1}{\gamma} \ln p - \ln \rho + C, \quad (A.80)$$

where

$$C = \frac{R}{c_p} \ln p_0 - \ln R. \tag{A.81}$$

Nondimensionalizing (A.80), by the use of (A.30) and (A.31), we obtain

$$\ln \theta_* = \frac{1}{\gamma} \ln \left(p_s + \rho_s U f_0 L p \right) - \ln \left[\rho_s \left(1 + \epsilon F \rho \right) \right] + C =$$

$$= \frac{1}{\gamma} \ln \left[p_s \left(1 + \frac{\rho_s U f_0 L p}{p_s / r h o_s} \right) \right] - \ln \rho_s - \ln \left(1 + \epsilon F \rho \right) + C =$$

$$= \frac{1}{\gamma} \ln p_s + \frac{1}{\gamma} \ln \left[1 + \frac{U f_0 L p}{p_s / \rho_s} \right] - \ln \rho_s - \ln \left(1 + \epsilon F \rho \right) + C =$$

$$= \frac{1}{\gamma} \ln p_s - \ln \rho_s + \frac{1}{\gamma} \ln \left[1 + \epsilon \frac{f_0^2 L^2}{p_s / \rho_s} p \right] - \ln \left(1 + \epsilon F \rho \right) + C \approx$$

$$[Taylor series expansion] \approx \frac{1}{\gamma} \ln p_s - \ln \rho_s + \epsilon \frac{1}{\gamma} \frac{f_0^2 L^2}{p_s / \rho_s} p - \epsilon F \rho + O(\epsilon^2) + C. \tag{A.82}$$

By setting

$$\ln \theta_* = \theta_s \left[1 + \epsilon F \theta(x, y, z, t) \right], \tag{A.83}$$

where

$$ln\theta_s = \frac{1}{\gamma} \ln p_s - \ln \rho_s + C, \tag{A.84}$$

and expanding θ in an ϵ -series

$$\theta = \theta_0 + \epsilon \theta_1 + \epsilon^2 \theta_2 + \dots \tag{A.85}$$

(A.82) becomes

$$\ln\left[\theta_{s}(1+\epsilon F(\theta_{0}+\epsilon\theta_{1}))\right] = \frac{1}{\gamma}\ln p_{s} - \ln \rho_{s} + \epsilon \frac{1}{\gamma} \frac{f_{0}^{2}L^{2}}{p_{s}/\rho_{s}} (p_{0}+\epsilon p_{1}) - \epsilon F(\rho_{0}+\epsilon\rho_{1}) \iff \ln \theta_{s} - \epsilon F(\theta_{0}+\epsilon\theta_{1}) \approx \frac{1}{\gamma}\ln p_{s} - \ln \rho_{s} + \epsilon \frac{1}{\gamma} \frac{f_{0}^{2}L^{2}}{p_{s}/\rho_{s}} (p_{0}+\epsilon p_{1}) - \epsilon F(\rho_{0}+\epsilon\rho_{1}) \Rightarrow F\theta_{0} = \frac{1}{\gamma} \frac{f_{0}^{2}L^{2}}{p_{s}/\rho_{s}} p_{0} - F\rho_{0}. \quad (A.86)$$

Since

$$F = \frac{f_0^2 L^2}{gD},\tag{A.87}$$

we yield

$$\theta_0 = \frac{1}{\gamma} \left(\frac{\rho_s g D}{p_s} \right) p_0 - \rho_0. \tag{A.88}$$

From the hydrostatic and geostrophic approximation, we can rewrite θ_0 as

$$\theta_0 = -\frac{p_0}{\gamma p_s} \frac{\partial p_s}{\partial z} + \frac{1}{\rho_s} \frac{\partial}{\partial z} (\rho_s p_0) = \frac{\partial p_0}{\partial z} + \frac{p_0}{\rho_s} \frac{\partial \rho_s}{\partial z} - \frac{p_0}{\gamma p_s} \frac{\partial p_s}{\partial z}. \tag{A.89}$$

By noting that (A.84) is equivalent to

$$\theta_{s} = \frac{p_{s}^{\frac{1}{\gamma}}}{\rho_{s}} + C \Rightarrow \frac{\partial \theta_{s}}{\partial z} = \frac{\partial}{\partial z} \left(\frac{p_{s}^{\frac{1}{\gamma}}}{\rho_{s}} \right) \Rightarrow \dots \Rightarrow \frac{1}{\theta_{s}} \frac{\partial \theta_{s}}{\partial z} = \frac{1}{\gamma p_{s}} \frac{\partial p_{s}}{\partial z} - \frac{1}{\rho_{s}} \frac{\partial \rho_{s}}{\partial z}, \tag{A.90}$$

we can rewrite θ_0 as

$$\theta_0 = \frac{\partial p_0}{\partial z} - p_0 \frac{1}{\theta_s} \frac{\partial \theta_s}{\partial z}.$$
 (A.91)

However, if we make use of the observation that

$$\frac{1}{\theta_s} \frac{\partial \theta_s}{\partial z} \sim \mathcal{O}(\epsilon), \tag{A.92}$$

we obtain

$$\theta_0 = \frac{\partial p_0}{\partial z}.\tag{A.93}$$

Now, let us invoke (A.83) into the thermodynamic equation (A.21), i.e.,

$$\begin{split} \frac{D\theta_*}{Dt_*} &= \frac{\theta}{c_p T_*} \left(\frac{k}{\rho_*} \nabla^2 T_* + Q_* \right) \Longleftrightarrow \\ \frac{D\theta_s (1 + \epsilon F(\theta_0 + \epsilon \theta_1))}{D \left(\frac{L}{U} t \right)} &= \frac{\theta_s (1 + \epsilon F(\theta_0 + \epsilon \theta_1))}{c_p T} \left(\frac{k}{\rho_*} \nabla^2 T_* + Q_* \right) \Longleftrightarrow \\ \frac{U}{L} \left[\frac{D\theta_s}{Dt} (1 + \epsilon F(\theta_0 + \epsilon \theta_1)) + \theta_s \epsilon F \frac{D(\theta_0 + \epsilon \theta_1)}{dt} \right] &= \\ &= \frac{\theta_s (1 + \epsilon F(\theta_0 + \epsilon \theta_1))}{c_p T} \left(\frac{k}{\rho_*} \nabla^2 T_* + Q_* \right) \Longleftrightarrow \\ \frac{D\theta}{Dt} + \frac{w(1 + \epsilon F\theta)}{\epsilon F\theta_s} \frac{\partial \theta_s}{\partial z} &= \left[\epsilon = \frac{U}{f_0 L} \; ; \; F = \frac{f_0^2 L^2}{g D} \right] = \frac{\theta_*}{\theta_s} \left(\frac{\kappa_*}{c_p T_*} \right) \frac{g D}{U^2 f_0}, \end{split}$$
(A.94)

where

$$\kappa_* \equiv \frac{k}{\rho_*} \nabla^2 T_* + Q_*. \tag{A.95}$$

Pedlosky (1987) notes that for the atmosphere, $c_pT_* \sim \mathcal{O}(gD) \Rightarrow \kappa_* \leq \mathcal{O}(U^2f_0)$ and so we nondimensionalize κ_* as

$$\kappa = \kappa_* \frac{gD}{c_n T_* f_0 U^2}.\tag{A.96}$$

Since the vertical velocity can be expressed as $w = \epsilon w_1 + \epsilon^2 w_2 + ...$, we rewrite (A.94) as

$$\frac{\partial(\theta_0 + \epsilon \theta_1)}{\partial t} + (u_0 + \epsilon u_1) \frac{\partial(\theta_0 + \epsilon \theta_1)}{\partial x} + (v_0 + \epsilon v_1) \frac{\partial(\theta_0 + \epsilon \theta_1)}{\partial y} + \frac{(w_1 + \epsilon w_2)}{F\theta_s} \frac{\partial \theta_s}{\partial z} (1 + \epsilon F(\theta_0 + \epsilon \theta_1)) = (1 + \epsilon F(\theta_0 + \epsilon \theta_1))\kappa. \quad (A.97)$$

Thus, to lowest order we have

$$\frac{D\theta_0}{Dt} + w_1 \frac{1}{F\theta_s} \frac{\partial \theta_s}{\partial z} = \kappa. \tag{A.98}$$

We now define the stratification parameter, S(z), as

$$S(z) = \frac{1}{F\theta_s} \frac{\partial \theta_s}{\partial z} = \frac{N_s^2 D^2}{f_0^2 L^2} \sim \mathcal{O}(1), \tag{A.99}$$

and

$$N_s^2 = \frac{g}{D\theta_s} \frac{\partial \theta_s}{\partial z}.$$
 (A.100)

The heating rate κ can be considered small over the advective time scale, but in general, the $O(\epsilon)$ vertical motion is obtained from

$$w_1 = \left[\kappa - \frac{D_0 \theta_0}{Dt}\right] \frac{1}{S(z)}.\tag{A.101}$$

Hence, the vertical velocity is now described by the $\mathcal{O}(1)$ dynamical θ_0 -field and can be substituted into the right hand side of (A.67) to yield

$$\frac{1}{\rho_s} \frac{\partial(\rho_s w_1)}{\partial z} = \frac{1}{\rho_s} \frac{\partial}{\partial z} \left[\frac{\rho_s}{S(z)} \left(\kappa - \frac{D_0 \theta_0}{Dt} \right) \right] =
= \frac{1}{\rho_s} \frac{\partial}{\partial z} \left[\frac{\rho_s \kappa}{S(z)} \right] - \frac{1}{\rho_s} \frac{D_0}{Dt} \left[\frac{\partial}{\partial z} \left(\frac{\rho_s}{S(z)} \theta_0 \right) \right] + \frac{1}{S(z)} \left(\frac{\partial u_0}{\partial z} \frac{\partial \theta_0}{\partial x} + \frac{\partial v_0}{\partial z} \frac{\partial \theta_0}{\partial y} \right).$$
(A.102)

From the geostrophic approximation (A.52) and the hydrostatic approximation (A.93) the thermal wind relation can be established;

$$\begin{cases}
\frac{\partial v_0}{\partial z} = \frac{\partial \theta_0}{\partial x}, \\
\frac{\partial u_0}{\partial z} = -\frac{\partial \theta_0}{\partial y}.
\end{cases}$$
(A.103)

upon which the last term in (A.102) identically vanish. Thus, the vorticity equation (A.67) reduces to

$$\frac{D_0}{Dt} \left[\zeta_0 + \beta y + \frac{1}{\rho_s} \frac{\partial}{\partial z} \left(\frac{\rho_s(z)}{S(z)} \theta_0 \right) \right] = \frac{1}{\rho_s} \frac{\partial}{\partial z} \left[\frac{\rho_s(z)\kappa}{S(z)} \right]. \tag{A.104}$$

In the absence of a heating source, we can neglect the right hand side and thus obtain a conservation statement

$$\frac{D_0}{Dt} \left[\zeta_0 + \beta y + \frac{1}{\rho_s} \frac{\partial}{\partial z} \left(\frac{\rho_s(z)}{S(z)} \theta_0 \right) \right] = 0, \tag{A.105}$$

or, equivalently,

$$\frac{D_0 q}{Dt} = 0, (A.106)$$

where

$$q = \zeta_0 + \beta y + \frac{1}{\rho_s} \frac{\partial}{\partial z} \left(\frac{\rho_s(z)}{S(z)} \theta_0 \right). \tag{A.107}$$

The geostrophic and hydrostatic approximations allow us to express each dependent variable as $p_0 = \psi$, whereupon

$$\left[\frac{\partial}{\partial t} - \frac{\partial \psi}{\partial y}\frac{\partial}{\partial x} + \frac{\partial \psi}{\partial x}\frac{\partial}{\partial y}\right] \left[\frac{\partial^2 \psi}{\partial x^2} + \frac{\partial^2 \psi}{\partial y^2} + \frac{1}{\rho_s}\frac{\partial}{\partial z}\left(\frac{\rho_s(z)}{S(z)}\frac{\partial \psi}{\partial z}\right) + \beta y\right] = 0.$$
(A.108)

This is the governing equation of motion for a stratified fluid at large (synoptic) scales, the so-called quasi-geostrophic potential vorticity equation. It is completely written in terms of the $\mathcal{O}(1)$ pressure field or stream function. Once it has been determined, u_0 , v_0 , ρ_0 , θ_0 and w_1 follow directly.

A.6. Connecting the QGPV equation to Charney's theory

Charney (1971) derived an original theory on geostrophic turbulence following the conservation of the quantity he denoted pseudo-potential vorticity. The aim is to link (A.108) to Charney's theory. We start by noting that (A.108) can be written as

$$\frac{D_0}{Dt} \left[\nabla_H^2 \psi + \beta y + \frac{1}{\rho_s} \frac{\partial}{\partial z} \left(\frac{\rho_s(z)}{S(z)} \frac{\partial \psi}{\partial z} \right) \right] = 0, \tag{A.109}$$

and that

$$S(z) = \frac{1}{F\theta_s} \frac{\partial \theta_s}{\partial z} = \frac{N_s^2 D^2}{f_0^2 L^2},\tag{A.110}$$

which hence leads to

$$\frac{D_0}{Dt} \left[\nabla_H^2 \psi + \beta y + \frac{1}{\rho_s} \frac{\partial}{\partial z} \left(\frac{f_0^2 L^2}{N_s^2 D^2} \rho_s \frac{\partial \psi}{\partial z} \right) \right] = 0. \tag{A.111}$$

Expansion of the third term in (A.111) yields

$$\frac{1}{\rho_s} \frac{\partial}{\partial z} \left(\frac{f_0^2 L^2}{N_s^2 D^2} \rho_s \frac{\partial \psi}{\partial z} \right) = \frac{f_0^2 L^2}{N_s^2 D^2} \left(\frac{\partial^2 \psi}{\partial z^2} + \frac{1}{\rho_s} \frac{\partial \rho_s}{\partial z} \frac{\partial \psi}{\partial z} - \frac{2}{N_s} \frac{\partial N_s}{\partial z} \frac{\partial \psi}{\partial z} \right), \tag{A.112}$$

so that

$$\frac{D_0}{Dt} \left[\nabla_H^2 \psi + \frac{f_0^2 L^2}{N_s^2 D^2} \left(\frac{\partial^2 \psi}{\partial z^2} + \frac{1}{\rho_s} \frac{\partial \rho_s}{\partial z} \frac{\partial \psi}{\partial z} - \frac{2}{N_s} \frac{\partial N_s}{\partial z} \frac{\partial \psi}{\partial z} \right) \right] + \beta \frac{\partial \psi}{\partial x} = 0.$$
(A.113)

Introducing the Charney substitution

$$\psi = \left(\frac{\rho_0}{\rho_s}\right)^n \chi,\tag{A.114}$$

which is inserted into (A.113) to yield, after a little simplification,

$$\frac{D_0}{Dt} \left[\left(\frac{\rho_0}{\rho_s} \right)^n \nabla_H^2 \chi + \rho_0^n \frac{f_0^2 L^2}{N_s^2 D^2} \left[\frac{\partial \rho_s}{\partial z} \chi \left(\rho_s^{-n-1} \frac{2n}{N_s} \frac{\partial N_s}{\partial z} + \rho_s^{-n-2} n^2 \left(\frac{\partial \rho_s}{\partial z} \right)^2 \right) + \right. \\
\left. - n \rho_s^{-n-1} \frac{\partial^2 \rho_s}{\partial z^2} \chi - \rho_s^{-n} \frac{2}{N_s} \frac{\partial N_s}{\partial z} \frac{\partial \chi}{\partial z} + \rho_s^{-n-1} \left(1 - 2n \right) \frac{\partial \rho_s}{\partial z} \frac{\partial \chi}{\partial z} + \rho_s^{-n} \frac{\partial^2 \chi}{\partial z^2} \right] \right] + \\
+ \beta \left(\frac{\rho_0}{\rho_s} \right)^n \frac{\partial \chi}{\partial x} = 0. \quad (A.115)$$

Choosing $n = \frac{1}{2}$, we yield a convenient cancellation of the second term involving $\frac{\partial \chi}{\partial x}$. Rescaling the vertical coordinate as

$$\begin{cases}
\frac{\partial}{\partial z} \to \frac{N_s D}{f_0 L} \frac{\partial}{\partial Z}, \\
\frac{\partial^2}{\partial z^2} \to \frac{N_s^2 D^2}{f_0^2 L^2} \frac{\partial^2}{\partial Z^2} + \frac{N_s^2 D^2}{f_0^2 L^2} \frac{1}{N_s} \frac{\partial N_s}{\partial Z} \frac{\partial}{\partial Z},
\end{cases} (A.116)$$

we obtain, after multiplication by $\left(\frac{\rho_s}{\rho_0}\right)^{\frac{1}{2}}$ and using $n=\frac{1}{2}$,

$$\frac{D_0}{Dt} \left[\nabla_H^2 \chi + \frac{1}{4\rho_s^2} \left(\frac{\partial \rho_s}{\partial Z} \right)^2 \chi - \frac{1}{2\rho_s} \frac{\partial^2 \rho_s}{\partial Z^2} \chi + \frac{1}{2\rho_s} \frac{\partial \ln N_s}{\partial Z} \frac{\partial \rho_s}{\partial Z} \chi \right]
- \frac{\partial \ln N_s}{\partial Z} \frac{\partial \chi}{\partial Z} + \frac{\partial^2 \chi}{\partial Z^2} + \beta \frac{\partial \chi}{\partial Z} = 0. \quad (A.117)$$

Assuming that the atmospheric density profile can be approximated as (for example, this choice is arbitrary and does not influence the validity of the theory);

$$\rho_s = \rho_0 e^{-\frac{f_0 L}{DN_s} Z},\tag{A.118}$$

we obtain

$$\frac{D_0}{Dt} \left[\nabla_3^2 \chi - \frac{\partial \ln N_s}{\partial z} \left(\frac{\partial \chi}{\partial Z} + \frac{1}{2} \frac{f_0 L}{N_s D} \chi \right) - \frac{1}{4} \frac{f_0^2 L^2}{N_s^2 D^2} \chi \right] + \beta \frac{\partial \chi}{\partial x} = 0. \quad (A.119)$$

Introducing the internal Rossby deformation radius

$$\lambda = \frac{N_s D}{f_0},\tag{A.120}$$

this can be simplified to

$$\frac{D_0}{Dt} \left[\nabla_3^2 \chi - \frac{\partial \ln N_s}{\partial z} \left(\frac{\partial \chi}{\partial Z} + \frac{L}{2\lambda} \chi \right) - \frac{L^2}{4\lambda^2} \chi \right] + \beta \frac{\partial \chi}{\partial x} = 0.$$
 (A.121)

A comparison with Charney (1971) shows that the governing equations are exactly the same except from the presence of the potential temperature θ instead of N_s . It is likely that this is just a typo in Charney (1971), which is supported by the subsequent assumption that the scale of variation of N_s is larger than the vertical scale of the turbulence, upon which terms involving the vertical gradient of N_s are neglected. Note however, that the assumption that the vertical scale of variation of lnN_s is smaller than the vertical scale of the turbulence, is a weaker assumption. In addition, Charney neglected the β -term by noting that advection of relative vorticity dominates over the advection of the Earth's vorticity. Charney also made the assumption that $\mathcal{O}(L) < \mathcal{O}(2\lambda)$ and hence neglected the potential term. However, for completeness, we will keep both the potential and the β -term in the following. Thus,

$$\frac{D_0}{Dt} \left[\nabla_3^2 \chi - \frac{L^2 \chi}{4\lambda^2} \right] + \beta \frac{\partial \chi}{\partial x} \approx 0. \tag{A.122}$$

where the total derivative is given by

$$\frac{D_0}{Dt} = \frac{\partial}{\partial t} + e^{\frac{L}{2\lambda}Z} \left(\frac{\partial \chi}{\partial x} \frac{\partial}{\partial y} - \frac{\partial \chi}{\partial y} \frac{\partial}{\partial x} \right)$$
(A.123)

where use have been made of (A.114) and (A.118). Since Charney assumed that $\mathcal{O}(L) < \mathcal{O}(2\lambda)$, the exponential term multiplying the advective operator vanishes.

We now wish to examine the time evolution of energy and enstrophy. By multiplying (A.122) by $\rho_s \chi$ we obtain

$$\rho_s \chi \left[\frac{\partial}{\partial \tau} + \left(\frac{\partial \chi}{\partial x} \frac{\partial}{\partial y} - \frac{\partial \chi}{\partial y} \frac{\partial}{\partial x} \right) \right] \left[\nabla_3^2 \chi - \frac{L^2 \chi}{4\lambda^2} \right] = 0. \tag{A.124}$$

The first term can be rewritten as

$$\rho_s \chi \frac{\partial}{\partial \tau} \left[\nabla_3^2 \chi - \frac{L^2 \chi}{4\lambda^2} \right] = \rho_s \chi \nabla_3^2 \frac{\partial \chi}{\partial \tau} - \rho_s \frac{L^2}{4\lambda^2} \chi \frac{\partial \chi}{\partial \tau}. \tag{A.125}$$

Omitting the subscript 3 for the three-dimensional Laplacian and noting that

$$\begin{cases}
\nabla \cdot \left[\chi \nabla \frac{\partial \chi}{\partial \tau} \right] = \chi \nabla^2 \frac{\partial \chi}{\partial \tau} + \nabla \chi \cdot \nabla \frac{\partial \chi}{\partial \tau}, \\
\frac{\partial}{\partial \tau} \frac{(\nabla \chi)^2}{2} = \nabla \chi \cdot \nabla \frac{\partial \chi}{\partial \tau},
\end{cases} (A.126)$$

the first term (A.125) can be rewritten as

$$\rho_s \left(\nabla \cdot \left[\chi \nabla \frac{\partial \chi}{\partial \tau} \right] - \frac{\partial}{\partial \tau} \frac{\left(\nabla \chi \right)^2}{2} - \frac{L^2}{8\lambda^2} \frac{\partial \chi^2}{\partial \tau} \right). \tag{A.127}$$

The second term in (A.124) can be rewritten as

$$\rho_{s}\chi\left(\frac{\partial\chi}{\partial x}\frac{\partial}{\partial y} - \frac{\partial\chi}{\partial y}\frac{\partial}{\partial x}\right)\left(\nabla_{3}^{2}\chi - \frac{L^{2}\chi}{4\lambda^{2}}\right) =$$

$$= \rho_{s}\chi\left(\frac{\partial\chi}{\partial x}\frac{\partial}{\partial y}\nabla^{2}\chi - \frac{\partial\chi}{\partial y}\frac{\partial}{\partial x}\nabla^{2}\chi\right). \quad (A.128)$$

This can be reformulated by the use of the following observation;

$$\nabla \cdot \left(\boldsymbol{u} \chi \nabla^2 \chi \right) = \frac{\partial}{\partial x} \left(-\frac{\partial \chi}{\partial y} \chi \nabla^2 \chi \right) + \frac{\partial}{\partial y} \left(\frac{\partial \chi}{\partial x} \chi \nabla^2 \chi \right) = \dots = \chi \left(\boldsymbol{u} \cdot \nabla \right) \nabla^2 \chi, \tag{A.129}$$

upon which (A.124) can be written as

$$\rho_s \frac{\partial}{\partial \tau} \left[\frac{(\nabla \chi)^2}{2} + \frac{L^2}{8\lambda^2} \chi^2 \right] - \rho_s \nabla \cdot \left[u \chi \nabla^2 \chi + \chi \nabla \frac{\partial \chi}{\partial \tau} \right] = 0.$$
 (A.130)

Integration of (A.130) over a normalized cubic volume L^3 yields

$$\frac{1}{L^{3}} \int \int \int \left[\rho_{s} \frac{\partial}{\partial \tau} \left[\frac{(\nabla \chi)^{2}}{2} + \frac{L^{2}}{8\lambda^{2}} \chi^{2} \right] - \right] - \rho_{s} \nabla \cdot \left[\mathbf{u} \chi \nabla^{2} \chi + \chi \nabla \frac{\partial \chi}{\partial \tau} \right] \right] L dx \ L dy \ \frac{f_{0}L}{N_{s}D} dZ = 0. \iff$$

$$\frac{\partial}{\partial \tau} \int \int \int \frac{\rho_{s}}{2\lambda} \left[(\nabla \chi)^{2} + \frac{L^{2}}{4\lambda^{2}} \chi^{2} \right] dx \ dy \ dZ +$$

$$- \int \int \int \int \frac{\rho_{s}}{\lambda} \nabla \cdot \left[\mathbf{u} \chi \nabla^{2} \chi + \chi \nabla \frac{\partial \chi}{\partial \tau} \right] dx \ dy \ dZ = 0. \iff$$

$$\frac{\partial}{\partial \tau} \int \int \int \frac{\rho_{s}}{2\lambda} \left[(\nabla \chi)^{2} + \frac{L^{2}}{4\lambda^{2}} \chi^{2} \right] dx \ dy \ dZ - \int \int \int \frac{\rho_{s}}{\lambda} \nabla \cdot \mathbf{J} \ dx \ dy \ dZ = 0.$$
(A.131)

Making use of the divergence theorem and multiplying by λ , this can be rewritten as

$$\frac{\partial}{\partial t} \int \int \int \frac{\rho_s}{2} \left[(\nabla \chi)^2 + \frac{L^2}{4\lambda^2} \chi^2 \right] dx \ dy \ dZ - \oiint \rho_s \boldsymbol{J} \cdot \hat{\boldsymbol{n}} \ dA = 0. \quad (A.132)$$

The closed integral vanishes and we obtain

$$\int \int \int \frac{\rho_s}{2} \left[(\nabla \chi)^2 + \frac{L^2}{4\lambda^2} \chi^2 \right] dx \ dy \ dZ = const. \iff$$

$$\int \int \int \frac{\rho_s}{2} \left(\left[\left(\frac{\partial \chi}{\partial x} \right)^2 + \left(\frac{\partial \chi}{\partial y} \right)^2 \right] + \left[\left(\frac{\partial \chi}{\partial Z} \right)^2 + \xi^2 \chi^2 \right] \right) \ dx \ dy \ dZ = const.,$$
(A.133)

where

$$\xi \equiv \frac{L}{2\lambda}.\tag{A.134}$$

The first bracketed term in (A.133) corresponds to the kinetic energy whereas the second bracketed term contains the available potential energy, APE. The major point here is that energy is conserved.

Now, let us examine the temporal evolution of enstrophy. We begin by

multiplying (A.122) by $(\nabla^2 \chi - \xi^2 \chi)$, thus obtaining

$$\left(\nabla^{2}\chi - \xi^{2}\chi\right) \left[\frac{\partial}{\partial \tau} + \left(\frac{\partial \chi}{\partial x}\frac{\partial}{\partial y} - \frac{\partial \chi}{\partial y}\frac{\partial}{\partial x}\right)\right] \left[\nabla^{2}\chi - \frac{L^{2}\chi}{4\lambda^{2}}\right] = 0 \iff \frac{1}{2}\frac{\partial}{\partial \tau} \left(\nabla^{2}\chi - \xi^{2}\chi\right)^{2} + \left(\nabla^{2}\chi - \xi^{2}\chi\right) \left(\frac{\partial \chi}{\partial x}\frac{\partial}{\partial y} - \frac{\partial \chi}{\partial y}\frac{\partial}{\partial x}\right) \left(\nabla^{2}\chi - \xi^{2}\chi\right) = 0. \tag{A.135}$$

The second term can be rewritten as

$$\left(\nabla^{2}\chi - \xi^{2}\chi\right) \left(\frac{\partial\chi}{\partial x}\frac{\partial}{\partial y} - \frac{\partial\chi}{\partial y}\frac{\partial}{\partial x}\right) \left(\nabla^{2}\chi - \xi^{2}\chi\right) =
= \left(\nabla^{2}\chi - \xi^{2}\chi\right) \left(\boldsymbol{u}\cdot\nabla\right) \left(\nabla^{2}\chi - \xi^{2}\chi\right) = \left[\boldsymbol{\Phi} \equiv \nabla^{2}\chi - \xi^{2}\chi\right] =
= \boldsymbol{\Phi} \left(\boldsymbol{u}\cdot\nabla\right) \boldsymbol{\Phi} = \left(\boldsymbol{u}\cdot\nabla\right) \frac{\boldsymbol{\Phi}^{2}}{2} = \dots = \nabla\cdot\boldsymbol{u} \left[\frac{1}{2}\boldsymbol{\Phi}^{2}\right] \quad (A.136)$$

Thus, (A.135) can be reformulated as

$$\frac{1}{2}\frac{\partial}{\partial \tau}\Phi^2 + \nabla \cdot \boldsymbol{u} \left[\frac{1}{2}\Phi^2 \right] = 0. \tag{A.137}$$

Defining the potential enstrophy as

$$Q \equiv \frac{1}{2}\Phi^{2} = \frac{1}{2}\left(\nabla^{2}\chi - \xi^{2}\chi\right)^{2},$$
 (A.138)

we obtain

$$\frac{\partial Q}{\partial t} + \nabla \cdot (\boldsymbol{u}Q) = 0. \tag{A.139}$$

Normalized triple integration yields

$$\frac{1}{L^{3}} \int \int \int \left(\frac{\partial Q}{\partial \tau} + \nabla \cdot (\mathbf{u}Q) \right) L dx L dy \frac{L}{\lambda} Z = 0. \iff
\frac{\partial}{\partial \tau} \int \int \int \frac{1}{\lambda} Q dx dy dZ + \oiint \frac{1}{\lambda} Q \mathbf{u} \cdot \hat{\mathbf{n}} dA = 0. \Rightarrow
\int \int \int Q dx dy dZ = const. \quad (A.140)$$

Thus, both energy and enstrophy are conserved within the quasi-geostrophic framework when Charney assumptions have been implemented.

A.7. The role of the β -term

Up to now, we have not considered the possible role of the β -term in terms of quasi-geostrophic dynamics. One way to gain further insight is to study a simplified model such as the two-layer model. It is the most basic model in which baroclinic effects are present. Following Holton (2004), we start by

looking at the quasi-geostrophic potential vorticity equation, where we have restored the z-coordinate from Charney scaling.

$$\frac{\partial q}{\partial t} + (\mathbf{u_h} \cdot \nabla)q = 0, \tag{A.141}$$

where

$$q = \nabla_h^2 \psi + \lambda_d^{-2} \frac{\partial^2}{\partial z^2} \psi + f, \tag{A.142}$$

and

$$f = f_0 + \beta y \tag{A.143}$$

is the Coriolis parameter on a β -plane and

$$\lambda_d = \frac{ND}{f_0} \tag{A.144}$$

is the Rossby radius of deformation corresponding to a vertical scale D. We now separate the equation into two vertically separated layers so that

$$q_1 = f_0 + \beta y + \nabla_h^2 \psi_1 + \lambda_d^{-2} (\psi_2 - \psi_1), \tag{A.145}$$

and

$$q_2 = f_0 + \beta y + \nabla_h^2 \psi_2 + \lambda_d^{-2} (\psi_1 - \psi_2), \tag{A.146}$$

where 1 and 2 denotes the upper and lower layer, respectively. The barotropic (denoted m) and baroclinic (denoted t) components can be defined as

$$\begin{cases} \psi_m \equiv \frac{\psi_1 + \psi_2}{2}, \\ \psi_t \equiv \frac{\psi_1 - \psi_2}{2}, \end{cases}$$

and equivalently

$$\begin{cases} q_m \equiv \frac{q_1 + q_2}{2}, \\ q_t \equiv \frac{q_1 - q_2}{2}. \end{cases}$$

Thus, the potential vorticity equations in each layer can be rewritten as

$$q_1 = \beta y + \nabla^2 (2\psi_m - \psi_2) - 2\lambda_d^{-2} \psi_t,$$
 (A.147)

and

$$q_2 = \beta y + \nabla^2 \psi_2 + 2\lambda_d^{-2} \psi_t, \tag{A.148}$$

and hence

$$q_m = \beta y + \nabla^2 \psi_m,$$

$$q_t = \nabla^2 \psi_t - 2\lambda_d^{-2} \psi_t.$$
(A.149)
(A.150)

$$q_t = \nabla^2 \psi_t - 2\lambda_d^{-2} \psi_t. \tag{A.150}$$

At this point we note that in the midlatitude atmosphere, there is climatologically a mean zonal flow. So it is convenient to linearise the equations about a uniform mean zonal wind state so that

$$\left\{ \begin{array}{l} \psi_m = -u_m y + \psi_m', \\ \psi_t = -u_t y + \psi_t', \end{array} \right.$$

where u_m is the mean zonal wind and u_t is the mean thermal wind;

$$\begin{cases} u_m \equiv \frac{u_1 + u_2}{2}, \\ u_t \equiv \frac{u_1 - u_2}{2}. \end{cases}$$

Substitutions into the vorticity equations and linearisation (neglecting products of perturbation quantities) for each layer yield

$$\left[\frac{\partial}{\partial t} + u_1 \frac{\partial}{\partial x}\right] (q_1 + q_1') + u_1' \frac{\partial q_1}{\partial x} + v_1' \frac{\partial q_1}{\partial y} = 0, \tag{A.151}$$

$$\[\frac{\partial}{\partial t} + u_2 \frac{\partial}{\partial x} \] (q_2 + q_2') + u_2' \frac{\partial q_2}{\partial x} + v_2' \frac{\partial q_2}{\partial y} = 0, \tag{A.152} \]$$

where q_1 and q_2 are given by (A.147) and (A.148) and

$$u_1 = u_m + u_t, \tag{A.153}$$

$$u_2 = u_m - u_t. (A.154)$$

Furthermore, it could be noted that

$$q_m = \beta y, \tag{A.155}$$

$$q_m' = \nabla^2 \psi_m', \tag{A.156}$$

$$q_t = 2\lambda_d^{-2} u_t y, \tag{A.157}$$

$$q_t' = \nabla^2 \psi_t' - 2\lambda_d^{-2} \psi_t'. \tag{A.158}$$

Summation, rearrangement and dropping the primes for the stream functions give eventually the evolution of the barotropic perturbation vorticity;

$$\left[\frac{\partial}{\partial t} + u_m \frac{\partial}{\partial x}\right] \nabla^2 \psi_m + \beta \frac{\partial \psi_m}{\partial x} + u_t \frac{\partial}{\partial x} \nabla^2 \psi_t = 0, \tag{A.159}$$

whereas subtraction gives the baroclinic evolution

$$\left[\frac{\partial}{\partial t} + u_m \frac{\partial}{\partial x}\right] \left(\nabla^2 \psi_t - 2\lambda_d^{-2} \psi_t\right) + \beta \frac{\partial \psi_t}{\partial x} + u_t \frac{\partial}{\partial x} \left(\nabla^2 \psi_m + 2\lambda_d^{-2} \psi_m\right) = 0.$$
(A.160)

In the simplest case, we study wave-like solutions of the form

$$\psi_m = Ae^{ik(x-ct)},\tag{A.161}$$

$$\psi_t = Be^{ik(x-ct)},\tag{A.162}$$

which we substitute into (A.159) and (A.160) upon which we obtain (after dividing through by the exponential factors) a set of linear equations for the coefficients:

$$ik\left[(c-u_m)k^2+\beta\right]A-ik^3u_tB=0, \tag{A.163}$$

$$ik\left[(c-u_m)(k^2+2\lambda_d^{-2})+\beta\right]B - iku_t(k^2-2\lambda_d^{-2})A = 0,$$
 (A.164)

which gives us nontrivial solutions only if the determinant is zero and hence we obtain a dispersion relation for c:

$$(c - u_m)^2 k^2 (k^2 + 2\lambda_d^{-2}) + 2(c - u_m)\beta(k^2 + \lambda_d^{-2}) + \beta^2 + u_t^2 k^2 (2\lambda_d^{-2} - k^2) = 0,$$
(A.165)

from which the phase speed can be obtained as (see Holton, 2004):

$$c = u_m - \frac{\beta(k^2 + \lambda_d^{-2})}{k^2(k^2 + 2\lambda_d^{-2})} \pm \delta^{\frac{1}{2}}, \tag{A.166}$$

where

$$\delta = \frac{\beta^2 \lambda_d^{-4}}{k^4 (k^2 + 2\lambda_d^{-2})^2} - \frac{u_t^2 (2\lambda_d^{-2} - k^2)}{k^2 + 2\lambda_d^{-2}}.$$
 (A.167)

It is immediately apparent that if $\delta < 0$, we will obtain solutions that grow in time. If we consider the case when $\beta = 0$, we find that $\delta < 0$ if $k^2 < 2\lambda_d^{-2}$. Thus, we can conclude that long waves are sensitive to perturbations and will tend to grow with time. Furthermore, a greater Rossby radius decreases the critical wave number at which perturbations start to grow according to this simple model. The main question of this chapter is the role of the β -effect. Already in (A.167) it is clear that for $\beta > 0$ and everything but the thermal wind kept constant, the role of the β -effect is to stabilize the flow. Thus, for perturbations to grow, the vertical wind shear (reflected in u_t) must increase for instabilities to develop. It can also be noted that in the absence of a vertical wind shear we only obtain free oscillations upon a barotropic flow with a phase speed for the barotropic perturbation that corresponds to that for a barotropic Rossby wave, i.e.,

$$c = u_m - \frac{\beta}{k^2}.\tag{A.168}$$

How is the β -effect expected to manifest itself in our simulations? According to Vallis (2006), we could expect an inverse energy transfer that is deflected into the $k_x = 0$ -mode so that the flow becomes more zonal. We could also, depending on the strength of the β -effect and hence at which length-scales its presence is felt, expect Rossby waves to develop. Thus, if there is a wide enough region in k-space between the so-called Rhines scale and the scale at which the friction dominates, waves would dominate the flow rather than geostrophic turbulence itself, in this particular range.

Bibliography

- Bartello, P. & Warn, T. 1996 Self-similarity of decaying two-dimensional turbulence J. Fluid Mech., 326, 357.
- BATCHELOR, G. K. 1969 Computation of the energy spectrum in homogeneous twodimensional turbulence *Phys. Fluids Suppl. II*, **12**, 233.
- BOFFETTA, G., CELANI, A. & VERGASSOLA, M. 2000 Inverse energy cascade in twodimensional turbulence: deviations from Gaussian behavior *Phys. Rev. E.*, **61**,
- BOFFETTA, G. 2007 Energy and enstrophy fluxes in the double cascade of two-dimensional turbulence J. Fluid Mech., 589, 253.
- BOFFETTA, G. & MUSACCHIO, S. 2010 Evidence for the double cascade scenario in two-dimensional turbulence *Phys. Rev. E*, **82**, 016307.
- VAN BOKHOVEN, L. J. A., TRIELING, R. R., CLERCX, H. J. H. & VAN HEIJST, G. J. F. 2007 Influence of initial conditions on decaying two-dimensional turbulence *Phys. Fluids*, **19**, 046601.
- BORUE, V. 1994 Inverse energy cascade in stationary two-dimensional homogeneous turbulence *Phys. Rev. Letters*, **72**, 1475.
- Bos, W. J. T. & Bertoglio, J.-P. 2009 Large-scale bottleneck effects in two-dimensional turbulence J. Turb., 10, 1.
- Bracco, A. & McWilliams, J. 2010 Reynolds-number dependency in homogeneous, stationary two-dimensional turbulence *J. Fluid Mech.*, **646**, 517.
- Carnevale, G. F., McWilliams, J. C., Pomeau, Y., Weiss, J. B. & Young, W. R. 1991 Evolution of vortex statistics in two-dimensional turbulence *Phys. Rev. Letters*, **66**, 2735.
- Charney, J. G. 1971 Geostrophic turbulence J. Atm. Sci., 28, 1087.
- Chen, S., Ecke, R. E., Eyink, G. L., Rivera, M., Wang, X. & Xiao, Z. 2006 Physical mechanism of the two-dimensional inverse energy cascade *Phys. Rev. Letters*, **96**, 084502.
- Clercx, H. J. H. & van Heijst, G. J. F. 2009 Two-dimensional Navier-Stokes turbulence in bounded domains *Appl. Mech. Rev.*, **62**, 020802.
- Danilov, S. & Gurarie, D. 2000 Quasi-two-dimensional turbulence Physics-Uspekhi, 43, 863.
- Danilov, S. & Gurarie, D. 2001a Forced two-dimensional turbulence in spectral and physical space *Phys. Rev. E*, **63**, 061208.

- DANILOV, S. & GURARIE, D. 2001b Nonuniversal features of forced two-dimensional turbulence in the energy range *Phys. Rev. E*, **63**, 020203-1.
- Danilov, S. & Gurarie, D. 2004 Scaling, spectra and zonal jets in beta-plane turbulence $Phys.\ Fluids,\ 16,\ 2592.$
- DRITSCHEL, D. G. 1995 A general theory for two-dimensional vortex interactions *J. Fluid Mech.*, **293**, 269.
- DRITSCHEL, D. G., TRAN, C. V. & SCOTT, R. 2007 Revisiting Batchelor's theory of two-dimensional turbulence *J. Fluid Mech.*, **591**, 379.
- ELHMAIDI, D., VON HARDENBERG, J. & PROVENZALE, A. 2005 Large scale dissipation and filament instability in two-dimensional turbulence *Phys. Rev. Lett.*, **95**, 014503-1.
- FALKOVICH, G. 1994 Bottleneck phenomenon in developed turbulence *Phys. Fluids*, **6**, 1411.
- FRISCH, U. 1991 From global scaling, a la Kolmogorov, to local multifractal scaling in fully developed turbulence *Proc. R. Soc. Lond. A*, **434**, 89.
- Frisch, U. 1995 Turbulence Cambridge University Press, Cambridge, UK.
- GAGE, K. S. & NASTROM, G. D. 1986 Theoretical interpretation of atmospheric wave number spectra of wind and temperature observed by commercial aircraft during GASP *J. Atm. Sci.*, **43**, 729.
- GILBERT, A. D. 1988 Spiral structures and spectra in two-dimensional turbulence J. Fluid Mech., 193, 475.
- VON HARDENBERG, J., McWilliams, J. C., Provenzale, A., Shchepetkin, A. & Weiss, J. B. 2000 Vortex merging in quasi-geostrophic flows *J. Fluid Mech.*, **412**, 331.
- Holton, J. R. 2004 An introduction to dynamic meteorology: 4th edition *Elsevier Academic Press*.
- Hua, B. L. & Haidvogel, D. B. 1986 Numerical simulations of the vertical structure of quasi-geostrophic turbulence *J. Atm. Sci.*, **43**, 2923.
- Kaneda, Y. & Ishihara, T. 2001 Nonuniversal k^{-3} energy spectrum in stationary two-dimensional homogeneous turbulence *Phys. Fluids*, **13**, 1431.
- KRAICHNAN, R. H. 1967 Inertial ranges in two-dimensional turbulence Phys. Fluids, 10, 1417.
- Kraichnan, R. H. 1971 Inertial-range transfer in two- and three-dimensional turbulence J. Fluid Mech., 47, 525.
- Kraichnan, R. H. 1974 On Kolmogorov's inertial-range theories *J. Fluid Mech.*, **62**, 305.
- Kukharkin, N. & Orszag, S. A. 1996 Generation and structure of Rossby vortices in rotating fluids *Phys. Rev. E*, **54**, 4524.
- LANDAU, L. D. & LIFSHITZ, E. M. 1987 Fluid Mechanics, Second edition *Pergamon Press*, **6** 140.
- Legras, B., Santangelo, P., & Benzi, R. 1988 High-resolution numerical experiments for forced two-dimensional turbulence *Europhys. Lett.*, 5, 37.
- Leith, C. E. 1968 Diffusion approximation for two-dimensional turbulence *Phys. Fluids*, **11**, 671.
- LILLY, D. K. 1983 Stratified turbulence and the mesoscale variability of the atmosphere J. Atm. Sci., 40, 749.

- LINDBORG, E. 1999 Can the atmospheric kinetic energy spectrum be explained by two-dimensional turbulence? *J. Fluid Mech.*, **388**, 259.
- LINDBORG, E. & ALVELIUS, K. 2000 The kinetic energy spectrum of the twodimensional enstrophy turbulence cascade *Phys. Fluids*, **12**, 945.
- LINDBORG, E. 2006 The energy cascade in a strongly stratified fluid *J. Fluid Mech.*, **550**, 207.
- MALTRUD, M. E. & VALLIS, G. K. 1991 Energy spectra and coherent structures in forced two-dimensional and beta-plane turbulence *J. Fluid Mech.*, **228**, 321.
- Maltrud, M. E. & Vallis, G. K. 1993 Energy and enstrophy transfer in numerical simulations of two-dimensional turbulence *Phys. Fluids A*, **5**, 1760.
- MCWILLIAMS, J. C. 1984 The emergence of isolated coherent vortices in turbulent flow J. Fluid Mech., 146, 21.
- McWilliams, J. 1989 Statistical properties of decaying geostrophic turbulence *J. Fluid Mech.*, **198**, 199.
- MCWILLIAMS, J. 1990 The vortices of two-dimensional turbulence *J. Fluid Mech.*, **219**, 361.
- McWilliams, J., Weiss, J. B. & Yavneh, I. 1999 The vortices of homogeneous geostrophic turbulence *J. Fluid Mech.*, **401**, 1.
- NASTROM, G. D. & GAGE, K. S. 1985 A climatology of atmospheric wave number spectra of wind and temperature observed by commercial aircraft *J. Atm. Sci.*, **42**, 950.
- Pasquero, C. & Falkovich, G. 2002 Stationary spectrum of vorticity cascade in two-dimensional turbulence *Phys. Rev. E*, **65**, 056305.
- Pedlosky, J. 1987 Geophysical fluid dynamics: 2nd edition Springer-Verlag New York.
- REINAUD, J. N., DRITSCHEL, D. G. & KOUDELLA, C. R. 2003 The shape of vortices in quasi-geostrophic turbulence *J. Fluid Mech.*, **474**, 175.
- RHINES, P. B. 1975 Waves and turbulence on a beta-plane J. Fluid Mech., 69, 417.
- RICHARDSON, L. F. 1922 Weather prediction by numerical process *Cambridge University Press*, Cambridge.
- Scott, R. K. 2007 Nonrobustness of the two-dimensional turbulent inverse cascade *Phys. Rev. E.*, **75**, 046301.
- SMITH, L. M. & YAKHOT, V. 1994 Finite-size effects in forced two-dimensional turbulence J. Fluid Mech., 274, 115.
- SMITH, K. S. 2004 A local model for planetary atmospheres forced by small-scale convection J. Atm. Sci., 61, 1420.
- Tabeling, P. 2002 Two-dimensional turbulence: a physicist approach *Physics Reports*, **362**, 1.
- Tran, C. V. & Bowman, J. C. 2004 Robustness of the inverse energy cascade in two-dimensional turbulence *Phys. Rev. E.*, **69**, 036303.
- Tran, C. V. & Dritschel, D. G. 2006 Vanishing enstrophy dissipation in twodimensional Navier-Stokes turbulence in the inviscid limit *J. Fluid Mech.*, **559**, 107
- Tulloch, R. & Smith, K. S. 2009 Quasigeostrophic turbulence with explicit surface dynamics: Application to the atmospheric energy spectrum *J. Atm. Sci.*, **66**, 450.

- Tung, K. K. & Orlando, W. W. 2003 The k^{-3} and $k^{-5/3}$ energy spectrum of atmospheric turbulence: quasigeostrophic two-level model simulation *J. Atm. Sci.*, **60**, 824.
- Vallis, G. K. & Maltrud, M. E. 1993 Generation of mean flows and jets on a beta plane and over topography *J. Phys. Ocean.*, **23**, 1346.
- Vallis, G. K. 2006 Atmospheric and oceanic fluid dynamics: fundamentals and large-scale circulation *Cambridge University Press*, Cambridge.
- Verma, M. K., Ayyer, A., Debliquy, O., Kumar, S. & Chandra, A. V. 2005 Local shell-to-shell energy transfer via nonlocal interactions in fluid turbulence *Pramana*, **65**, 297.